Dynamic and thermodynamic contribution to the October 2019 exceptional rainfall in West Central Africa

Kevin Kenfack[1*] · Francesco Marra[3] · Zéphirin Yepdo Djomou[1,2] · Lucie A. Djiotang Tchotchou[1] · Alain T. Tamoffo[4] · Derbetini A. Vondou[1]

[1]Laboratory for Environmental Modelling and Atmospheric Physics (LEMAP), Physics Department, University of Yaoundé 1, Yaoundé, Cameroon

[2]National Institute of Cartography, Cameroon

[3]Department of Geosciences, University of Padova, Italy

[4]Climate Service Center Germany (GERICS), Helmholtz-Zentrum Hereon, Fischertwiete 1, 20095 Hamburg, Germany

Corresponding author: **Kevin Kenfack**

Email: **kevinkenfack46@gmail.com**

ORCID: **0000-0003-1694-4906**

Kevin Kenfack's ORCID: 0000-0003-1694-4906

Francesco Marra's ORCID: 0000-0003-0573-9202

Lucie A. Djiotang Tchotchou's ORCID: 0000-0003-2860-428X

Alain T. Tamoffo's ORCID: 0000-0001-8482-8881

Derbetini A. Vondou's ORCID: 0000-0002-8681-5328

Abstract

Exceptional rainfall hit West Central Africa in October 2019. To understand the underlying mechanisms, we diagnosed the regional moisture and Moist Static Energy (MSE) budgets intending to highlight the importance of the dynamic and thermodynamic effects associated with this historic event. Analysis of the moisture budget reveals that the precipitation anomalies in October were mainly controlled by dynamic effects. Horizontal moisture advection induced by horizontal wind anomalies controls extreme precipitation north of West Central Africa, while vertical moisture advection induced by vertical velocity anomalies controls extreme precipitation south of West Central Africa. Changes in the thermodynamic effect, although not the key factor responsible for the events of October 2019, contribute up to 35% of the total effect on the northern part and 15% on the southern part of the domain. The residual term (6°N-14°N, 6°-20°E) is important and provides a caveat when estimating dynamic and thermodynamic processes. Diagnosis of the MSE balance averaged over the northern part of west Central Africa shows that the anomalous vertical motion is dominated by the dynamic effect, i.e. the wet enthalpy advection induced by the horizontal wind anomalies. This is confirmed by the high correlation (r = 0.6) between the two terms compared to the other terms. Whereas to the west of the Congo Basin, the increase in the net energy balance dominated the changes in vertical motion (r = 0.51). The horizontal advection of the MSE induced by the anomalies of the wet enthalpy and the vertical advection of the MSE induced by the anomalies of the MSE seem less important (r= 0.29 and -0.19 to the north and -0.17 and 0.03 to the south respectively). The strong anomalies in the MSE balance in the north are linked to its meridional component, in particular the meridional wind anomalies in the dynamic effect and the meridional anomalies in latent heat in the thermodynamic effect. Our results suggest that dynamic and thermodynamic effects should be jointly considered for adequately anticipating this kind of extreme event. Understanding the associated mechanisms could help us improve our projections and increase the region's population resilience to these extreme weather events.

Keywords: West Central Africa · Moisture budget · Moist static energy budget · Precipitation · wet enthalpy

1 Introduction

Equatorial Africa recorded unprecedented amounts of rainfall in October and November 2019 (Wainwright et al, 2020). Such a significant amount of precipitation is not without consequences for the population and the environment. In October, in most parts of East Africa in general, and in Kenya in particular, extreme rainfall led to flooding and landslides, provoking major destruction, with more than 100 deaths and around 18,000 people displaced internally and to neighbouring countries (http://floodlist.com/africa/kenya-floods-november-2019). In Central Africa, the Democratic Republic of Congo has been devastated by major flooding and forestry disruption along the Congo River, forcing many people to move (Gou et al. 2022). In the Central African Republic, extreme and persistent rainfall caused significant flooding and landslides, including the Oubangui River overflowing nearly 60 km of its coastline (Igri et al. 2023). In addition, the night of 27 to 28 October 2019 was disastrous in the West Cameroon region, mainly in the locality of Bafoussam where extreme rainfall for about 36 hours caused a landslide, resulting in significant material damage with 45 dead and others missing (Aretouyap et al. 2021; Mfondoum et al. 2021; Wantim et al. 2023). The episode was associated with a thermal depression over the Sahara and with anomalously high Sea Surface Temperatures (SST). The occurrence of these conditions may change in response to anthropogenic global warming, raising the question of whether devastating events such as the one of October 2019 could occur more frequently in the future (Nicholson et al. 2022). In particular, given that climate models predict an increasing trend in extreme rainfall in the region (Fotso-Nguemo et al. 2018, 2019; Sonkoué et al. 2018; Tamoffo et al. 2019, 2023) and that extreme precipitation in the region is associated with vegetation dynamics (Zhou et al. 2014; Mariotti et al. 2014; Marra et al. 2022; Garcin et al. 2018), it is crucial to understand the thermodynamic and dynamic mechanisms underlying these exceptional events of October 2019.

Recent studies have attempted to investigate the causes of extreme rainfall during the exceptional period of October 2019 in Equatorial Africa. Nicholson et al. (2022) showed that the heavy rainfall on the Guinean coast was reinforced by positive sea surface temperature anomalies along the Atlantic coast. This process leads to a significant advection of the moisture flux from the Atlantic, combined with the convergence of the moisture, which contributed to the increase in rainfall in the region (Pokam et al. 2011, Kuete et al. 2019). Wainwright et al. (2020) pointed out that the increase in rainfall over East Africa was a consequence of the positive phase of the Indian Ocean Dipole. Indeed, Black et al. (2005) reported that during periods of the year when the dipole mode index (DMI) IOD events are greater than 0.5°C over a period of 3 consecutive months and when the zonal SST gradient

is reversed over several months, the resulting increase in rainfall over East Africa is important. In addition, the positive IOD event of 2019 lasted from late summer through to December, influencing rainfall over East Africa.

Rainfall variability in Central Africa is highly dependent on the convergence of atmospheric moisture (Pokam et al. 2012; Washington et al., 2013; Dyer et al., 2017; Hua et al., 2019; Taguela et al. 2022). Under the effect of global warming, the increase in extreme precipitation is a consequence of the increase in available atmospheric humidity (Nicholson et al 2022). Although previous studies have focused on analyzing meteorological factors, there is still a general lack of knowledge about quantifying the dynamic and thermodynamic effects associated with these extremes of precipitation. In recent years, the decomposition of the water balance behind precipitation anomalies is often used to isolate the dynamic and thermodynamic contributions to extreme events (Li et al., 2017; Oueslati et al., 2019; Wen et al., 2022; Kenfack et al., 2023,2024). Water balance analysis has proved to be a useful tool for understanding anomaly fields in mean precipitation under the influence of global warming (Seager et al. 2014). Moist static energy (MSE), in particular, is a useful parameter for investigating the contribution of atmospheric moisture and analyzing vertical velocity (Wang and Li, 2020a, 2020b; Bell et a. 2015; Neelin, 2021; Nana et al. 2023; Andrews et al. 2023; Longandjo and Raoul, 2024; Kenfack et al. 2024). Recently, Kenfack et al. (2024) showed that, in the Congo Basin, the structure of the horizontal moisture advection anomalies is similar to that of the MSE advection anomalies during rainy seasons March-April-May (MAM) and September-October-November (SON). In addition, the atmospheric heating source has been identified as an indicator of precipitation (He et al. 2021). The increase in diabatic heating on the coast can contribute to the acceleration of near-surface winds (Pokam et al. 2014). An increase in this quantity implies an increase in latent warming, associated with a strong ocean-continent horizontal moisture gradient, which can lead to a strengthening of the boundary layer MSE, with a positive feedback process leading to extreme precipitation. Further, it has been demonstrated that a simultaneous reduction in the heating source and rainfall has been observed in reanalyses over recent decades in the Congo Basin (Kenfack et al. 2024). Given the highlighted importance of moisture, MSE and heating sources on rainfall variability, we adopt in this study an approach based on diabatic heating, water balance and MSE to diagnose dynamic and thermodynamic processes associated with the October 2019 rainfall extremes over West Equatorial Africa.

The remainder of the paper is structured as follows. A description of the observation and reanalysis data, and analysis methods is presented in Section 2. Section 3 describes the diabatic heating source and the performance of the reanalysis in capturing the October 2019 precipitation extremes. In Section 4, we investigate the dynamic and thermodynamic effects associated with the

moisture balance. The analysis of the dynamic and thermodynamic effects associated with the MSE budget during the October 2019 rainfall anomaly period over West Central Africa is presented in Section 5. Section 6 is conclusions and discussions.

2 Data and methods

2.1. Data

In this study, datasets from the fifth version of the European Centre for Medium-Range Weather Forecasts reanalysis, known as ERA5 (Hersbach et al., 2020), are used for the analyses. Johannsen et al. (2019) established that over equatorial Africa, ERA5 significantly improves over ERA-Interim (which represents the previous dataset), particularly in the description of the hydrological cycle. In addition, Cook and Vizy (2021) have shown that ERA5 represents well the spatial distribution of precipitation and atmospheric dynamic fields compared with previous generations, particularly over the Congo Basin. With a spatial resolution of 0.25°×0.25°, ERA5 is a global reanalysis dataset available from 1979 to the present, covering 137 pressure levels from the surface to 0.01 hPa. Monthly variables including horizontal and vertical wind components, geopotential, evaporation, humidity, heat flux and temperature are used in this study. For all variables, anomalies are obtained by removing the 30-year mean of the period 1988 to 2017. To assess ERA5's ability to detect October 2019 precipitation extremes, we used three observational datasets, including rain gauge products and gauge-adjusted satellite products: the Climate Hazards Group InfraRed Precipitation with Stations (CHIRPS) gridded dataset, available at a resolution of 0.05° × 0.05° (Funk et al., 2015); the Global Precipitation Climatology Project (GPCP-v2.2) with a grid spacing of 2.5° × 2.5° (Huffman et al., 2009); the Climatic Research Unit (CRU-TS4.03) gridded data at a resolution of 0.5° × 0.5° (Harris et al., 2020).

2.2 Methods

2.2.1 Diabetic heating

Apparent diabatic heating as proposed by Yanai and Tomita (1998) and Pokam et al. (2014) is defined as follows:

$$Q = \chi\left(\frac{\partial \theta}{\partial t} + u\frac{\partial \theta}{\partial x} + v\frac{\partial \theta}{\partial y} + \omega\frac{\partial \theta}{\partial p}\right) \quad (1)$$

$$\chi = c_p\left(\frac{T}{\theta}\right) \quad (2)$$

In equations 1 and 2, C_p (1,005 J Kg^{-1} K^{-1}) denotes the specific heat at constant pressure, θ is the potential temperature, ω is the vertical velocity (hPa s^{-1}), and $V=(u, v)$ is the vector of horizontal velocities. T (K) and p (hPa) represent the air temperature and the barometric pressure, respectively.

To quantify the monthly mean heating rate τ($K\,day^{-1}$) related to apparent heating, we use the relation:

$$\tau = \frac{Q}{c_p} \tag{3}$$

where Q is the combination of heat from radiation, latent heat from condensation and the convergence of vertical vortical transport of sensible heat.

2.2.2 Diagnosis of the moisture budget

The moisture budget used to quantify the contributions of evaporation and the horizontal and vertical components associated with the circulation of moist air in the atmosphere (Seager et al., 2010; Oueslati et al., 2019; Jiang et al., 2020; Moon and Ha, 2020; Wen et al., 2022; Zhao et al., 2022; Sheng et al., 2023; Kenfack et al., 2024) is defined as follows:

$$\langle \partial_t q \rangle + \langle V \cdot \nabla_h q \rangle + \langle \omega \cdot \partial_p q \rangle = E - P \tag{4}$$

In Eq. 4, q represents the specific humidity, $V=(u,v)$ denotes the horizontal wind and ω the vertical pressure velocity. E denotes surface evaporation and P precipitation. Angle brackets "⟨⟩" signify the mass integral from the surface (ps = 1000 hPa) to a pressure pt = 300 hPa, which represents the top of the atmosphere layer considered. The first term on the left of equation 4 can be neglected given its small variation over time on a monthly scale and could contribute to the residuals. To estimate the horizontal and vertical moisture advection components, we decompose equation 4 into its different linear and residual terms as follows:

$$P' = E' - \langle \nabla \cdot \nabla q' \rangle - \langle V' \cdot \nabla \bar{q} \rangle - \langle \bar{\omega} \partial_p q' \rangle - \langle \omega' \partial_p \bar{q} \rangle + Res \tag{5}$$

In Eq. 5, the overbar indicates the monthly mean climatology from 1988 to 2017 and primes indicate deviations from this climatology; The residual term "Res" contains the non-linear and transient processes associated with the joint variations in water vapor content and circulation. The terms $\langle -V' \cdot \nabla \bar{q} \rangle$ and $\langle -\omega' \partial_p \bar{q} \rangle$ represent the dynamic contributions (or effect) and refer to the moisture advection induced by the horizontal wind and by the vertical pressure velocity, respectively. The terms $\langle -\nabla \cdot \nabla q' \rangle$ and $\langle -\bar{\omega} \partial_p q' \rangle$ represent the thermodynamic contributions (or effect), and refer to the contribution of water vapor.

2.2.3 Diagnosis of the MSE budget

The MSE equation is defined as follows:

$$\langle \partial_t (c_v T + L_v T) \rangle + \langle V \cdot \nabla M \rangle + \langle \omega \partial_p m \rangle = F_{net} \quad (6)$$

where the moist enthalpy is

$$M = c_p T + L_v q \quad (7)$$

and the MSE is

$$m = c_p T + L_v q + \Psi \quad (8)$$

In equations 7 and 8, c_p (c_v) represents the specific heat at constant pressure (the specific heat at constant volume); T is the air temperature and Ψ the geopotential. F_{net} is the net energy entering the atmospheric column at the surface and top of the atmosphere (latent heat, sum of sensible heat, and shortwave and longwave radiative fluxes). Similar to the moisture flux equation, the first term on the left of equation 6 can be neglected given its small variation over time on a monthly scale and contributes to the residuals. In addition, it should be noted that variations in geopotential height along pressure levels are neglected in this formulation of the MSE budget. The remaining terms in equation 6 can be decomposed into horizontal and vertical advection components, as described by:

$$\langle \omega' \partial_p \bar{m} \rangle = -\langle \nabla \cdot \nabla M' \rangle - \langle V' \cdot \nabla \bar{M} \rangle - \langle \omega \partial_p m' \rangle + F'_{net} + Res \quad (9)$$

Anomalous vertical motion is analysed using this equation with a given profile of $\bar{m}$. Similar to the convention adopted for decomposing the moisture flux, the term $-\langle V' \cdot \nabla \bar{M} \rangle$ relates to the anomalous MSE associated with the atmospheric circulation and contains the dynamic contribution (or effect), while the two terms $-\langle \nabla \cdot \nabla M' \rangle$ and $-\langle \omega \partial_p m' \rangle$ refer to the thermodynamic contribution (or effect), which is crucial for diagnosing the thermal state of the atmosphere associated with the increase in the vertical rise of the air.

3 Diabatic heating and extreme rainfall

The increase in SSTs in the eastern Atlantic (Fig. 1a) is identified as one of the causes of the positive precipitation anomalies over western central Africa in October 2019. The warming contrast between the ocean and the continent favoured the strengthening of the moisture advection associated with the precipitation anomalies over West Central Africa (Fig. 1b). This is in agreement with Nicholson et al. (2022).

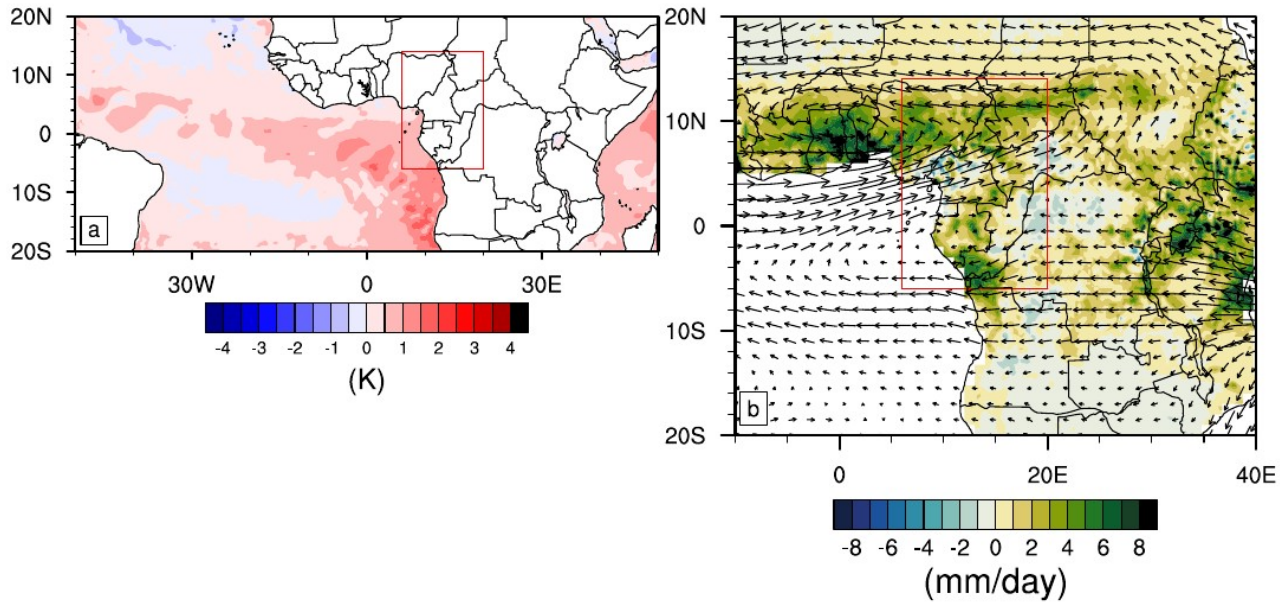

Fig 1. SST a) and rainfall b) anomalies during October 2019. The vectors represent anomalies of vertically integrated atmospheric moisture flux. The red box indicates the Central West Africa area.

Figure 2 represents the mean vertical profile (pressure-latitude) of diabatic heating averaged between 6° and 20°E during SON for the 1988-2017 climatology (Fig. 2a) and the corresponding profile for 2019 (Fig. 2b). During SON, the main source of heat is located between 3°S and 9°N for climatology, and between 5°S and 13°N for 2019.

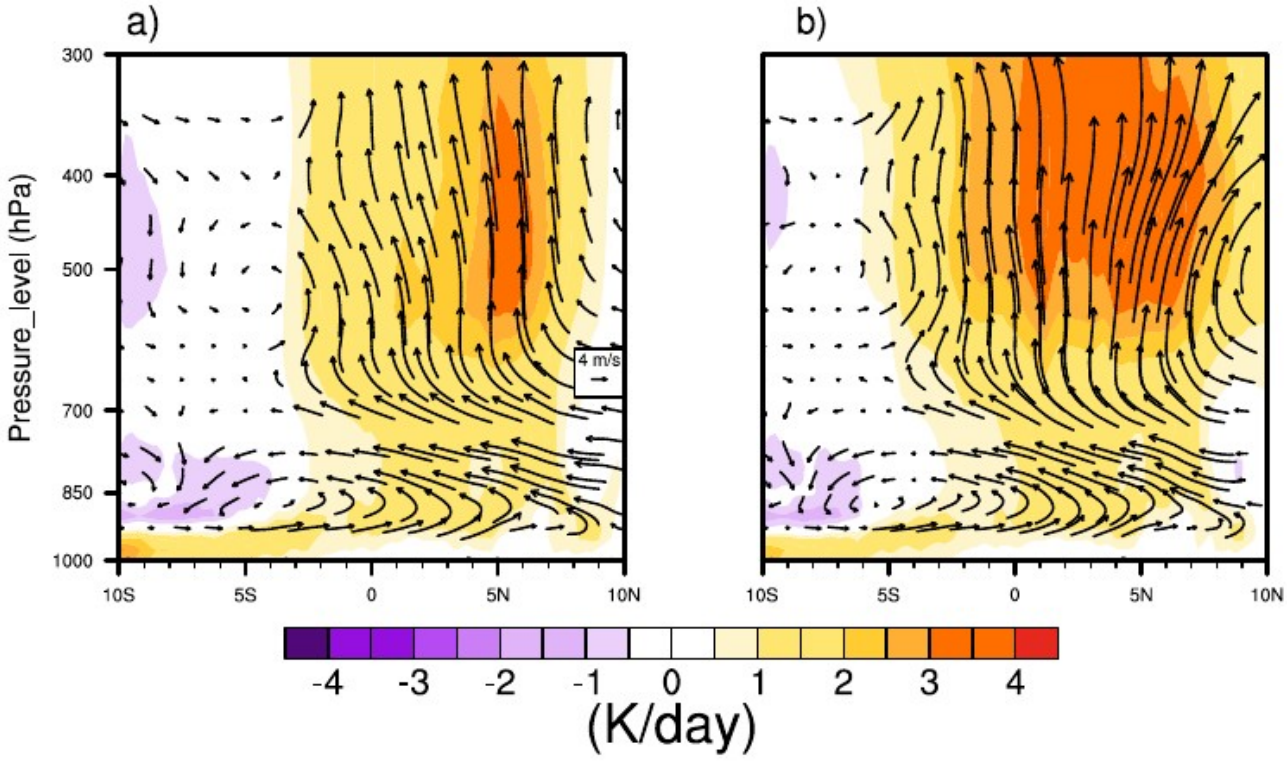

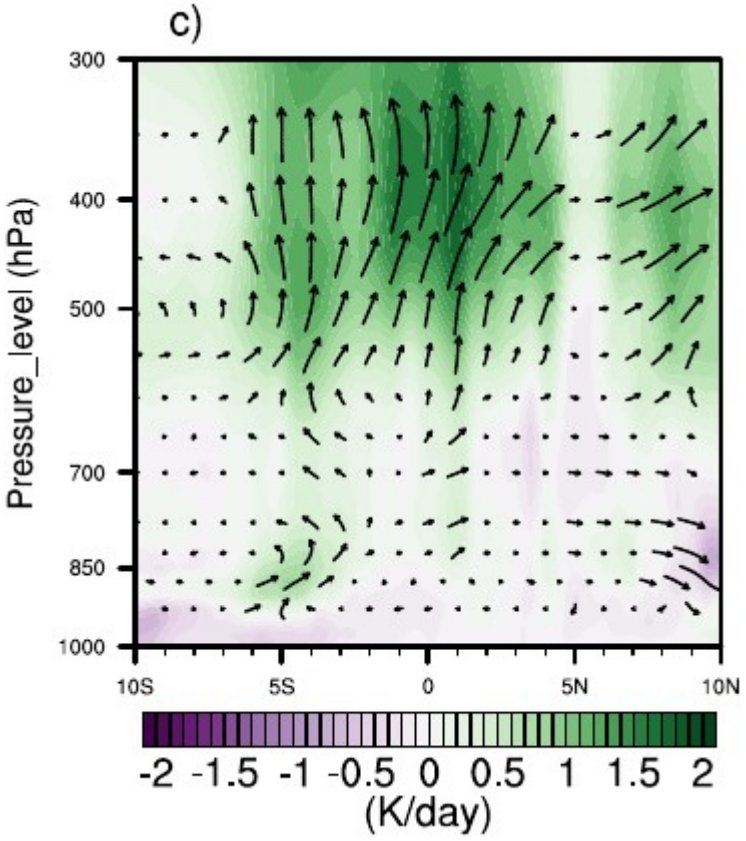

Fig 2. Diabatic heating and divergent meridional circulation (vectors; $m\,s^{-1}$) during the SON season for a) 1988-2017 avg, b) 2019 avg and c) the anomaly, all averaged between the 6° and 20°E. As the vertical velocity is much weaker than the meridional wind, its values have been enhanced by a factor of 600 for the clarity of the graph.

However, 2019 presents a more extensive and pronounced source of heat compared with the climatology 1988-2017. A 3-4 $K\,day^{-1}$ heating, more intense in 2019, occurred from 600 hPa. A cooling of 1- 2 $K\,day^{-1}$ took place around 850 hPa in the south and from 550 hPa in the north. The profound heating observed from 600 hPa originates at the surface on the southern portion of the domain (10°S). It is reinforced by the contrast between the large positive values and the negative values on either side of the equator between 500 and 400 hPa. The vertical structure of the divergent circulation is also illustrated in Figure 2. The divergent circulation appears more pronounced from 550 hPa in 2019 (Fig. 2b) compared with the climatology of 1988-2017 (Fig. 2a). This is consistent with the warming contrast observed. This uplift was reinforced by the warming of the equatorial Atlantic associated with an abnormally strong thermal low over the Sahara, which led to an acceleration of the dominant meridional flow in the divergent circulation (Fig. 2c). This is in

agreement with Nicholson et al. (2022), who highlighted that the West African monsoon was late to withdraw in 2019.

Although the SON season has shown significant diabatic heating compared to climatology, October 2019 in particular over West Central Africa recorded extremes of rainfall (Nicholson et al. 2022). In this study, we use the ERA5 reanalysis precipitation fields for water balance analysis. This ensures that all the examined physical quantities are consistent across the study. Before doing so, we assessed the performance of ERA5 in detecting the extreme precipitation events in October 2019. Figure 3 illustrates the interannual variability of October rainfall anomalies over West Central Africa for the period 1987-2021.

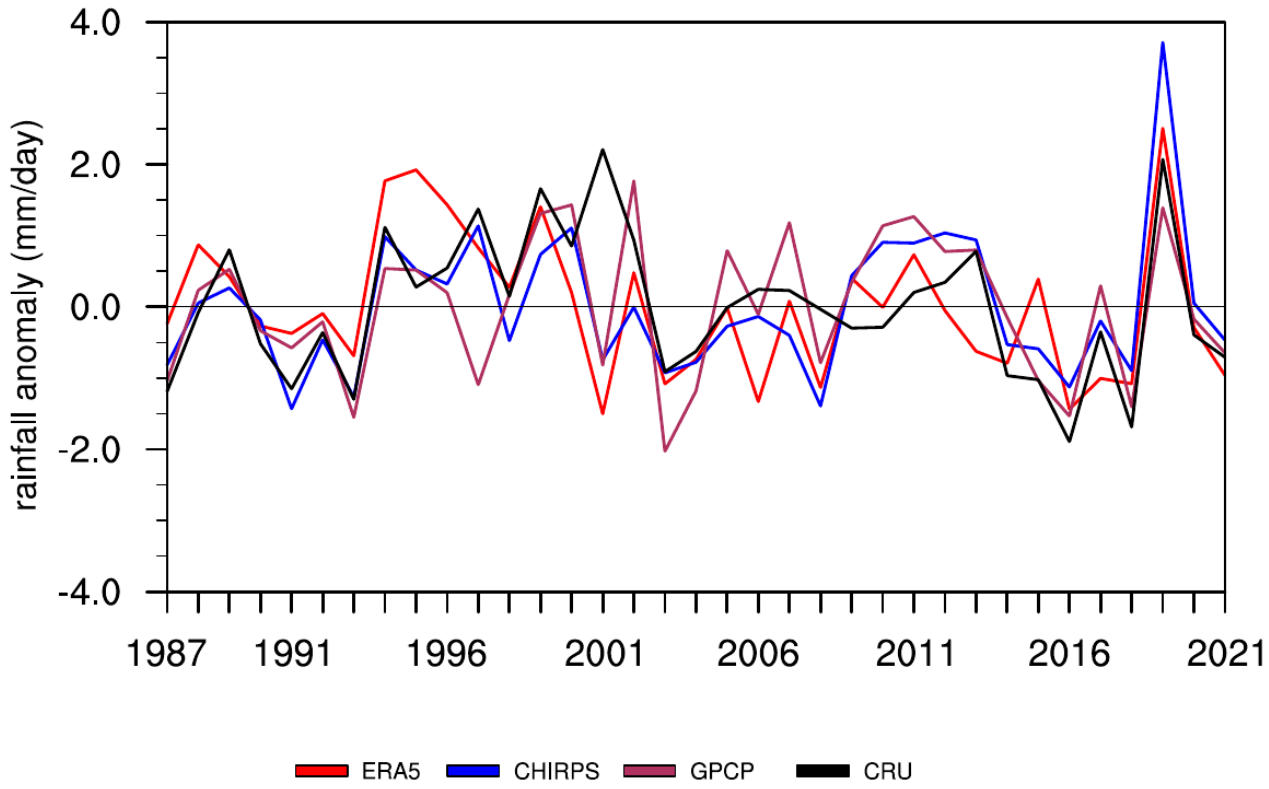

Fig 3. Temporal evolution of October rainfall anomaly over West Central Africa (6°S-14°N, 6°-20°E), from reanalysis data ERA5 (red) and from observational data CHIRPS (blue), GPCP (maroon) and CRU (black), covering the period 1987–2021.

The ERA5 reanalysis (red) and the CHIRPS (blue), GPCP (maroon) and CRU (black) observations are consistent in highlighting the high precipitation peak of 2019. CHIRPS shows the highest values of positive anomalies of up to 3.5 mm day^{-1}, while ERA5 shows values of up to 2.5 mm day^{-1}. Despite some differences between ERA5 and the observations in representing trends on an

interannual scale (Kenfack et al. 2024), the unprecedented event of October 2019 was well detected. In addition, the exceptional event is also detected by the MERRA2 reanalysis (Figure S1)

The increase in SSTs in the tropical Atlantic reached a record level in October 2019 (Nicholson et al. 2022). This may have resulted in an increased specific humidity over land. Figure 4 depicts the vertical profile (pressure level-latitude) of specific humidity (colors) and meridional wind (contours) averaged between 6° and 20°E for the 1988-2017 climatology (Fig. 4a), the October 2019 average (Fig. 4b), and the October 2019 anomaly (Fig. 4c).

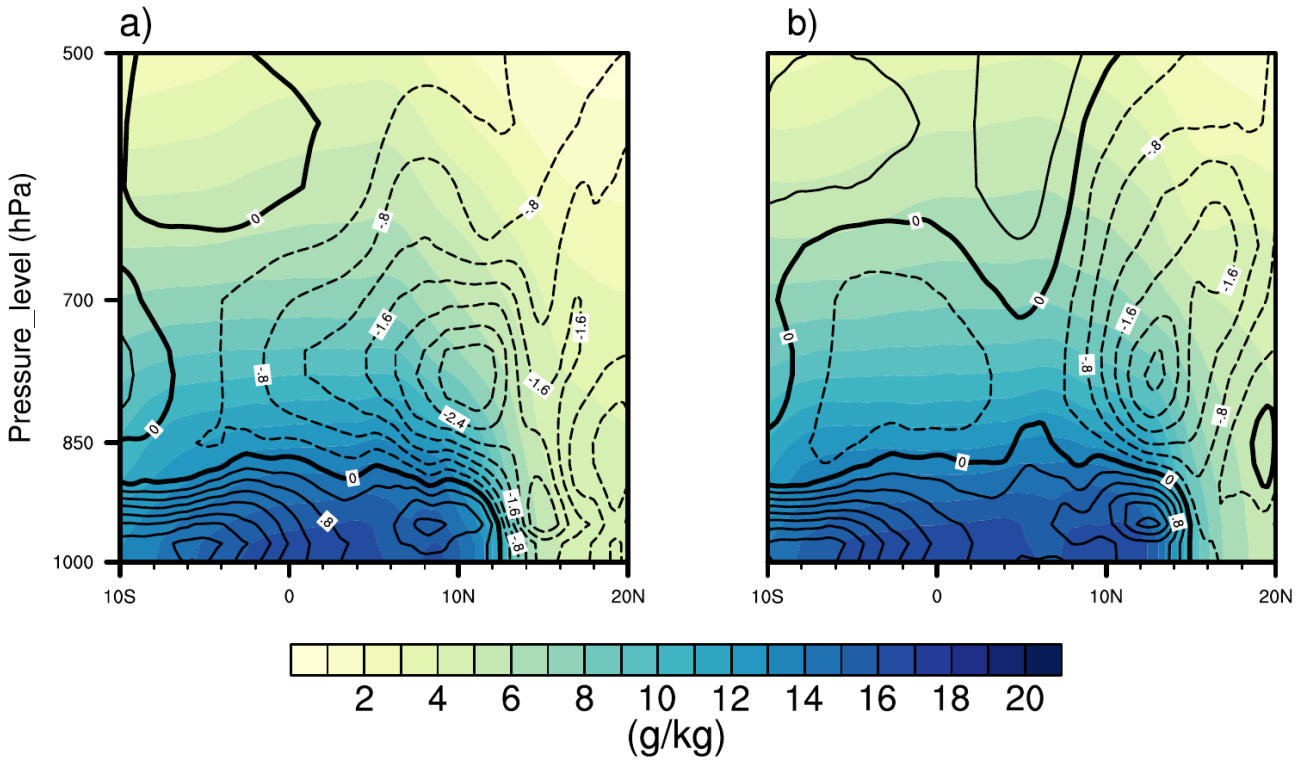

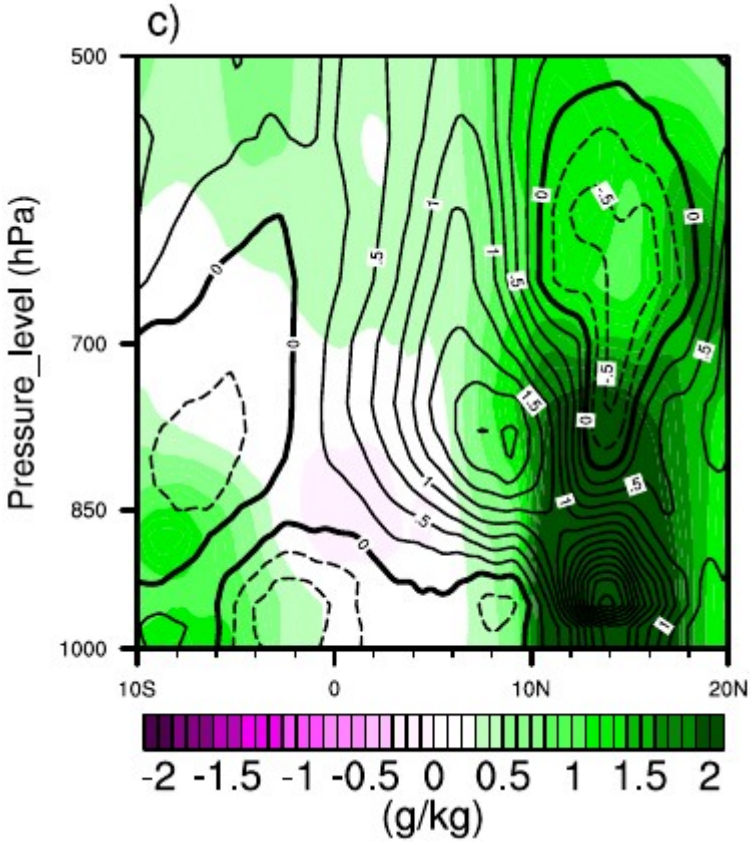

Fig. 4. Specific humidity and meridional wind (contours: m/s) in October for a) 1988-2017 avg, b) 2019 avg and c) the anomaly, averaged between 6°-20°E.

The 1988-2017 climatology is characterized by intense surface specific humidity extending as far as 12°N, whereas the October 2019 average appears to extend further to 15°N. In addition, the southerly wind in 2019 was more pronounced up to 15°N compared to the climatology. Analysis of the anomalies confirms that the humidity extended further north in West Central Africa in October 2019, compared with the climatology. The intensification of the southerly wind up to 15°N indicates that this moisture probably comes from the equatorial Atlantic. This is in agreement with Kamae et. al (2017), who highlighted that extreme precipitation can be a consequence of changes in humidity. Indeed, the increase in humidity associated with a substantial heating source contributes to an increase in precipitation. In addition, In the case of the monthly anomalies, the changes in the winds are thought to be a response to the increased moisture advection from the oceans as a result of global warming.

4 Moisture budget analysis

Rainfall variability in equatorial Central Africa is strongly dependent on the moisture inputs associated with atmospheric circulation (Jackson et al., 2009; Cook and Vizy, 2016, 2022; Dyer et al., 2017; Longandjo and Raoul, 2024). In the Congo Basin, atmospheric heating sources combined with the vertical advection of moisture induced by anomalous vertical motion are responsible for most of the interannual variability of precipitation (Kenfack et al., 2024). In this section, we decompose the moisture budget in equation 5 to examine the processes that led to the October 2019 extreme rainfall over West Central Africa. To do this, we analyse local variations in rainfall associated with atmospheric moisture introduced into the air column by atmospheric circulation.

The monthly anomalies of the different components of the water balance averaged over the northern part of west-central Africa (6°N-14°N, 6°-20°E) for the month of October 2019 (Fig. 5) indicate that the increase in dynamic processes dominated the increase in precipitation. Horizontal advection of moisture induced by the horizontal wind anomaly $\langle -V' \cdot \nabla \bar{q} \rangle$ was the most pronounced component (up to 2.5 mm/day). Although thermodynamic processes $\langle -\bar{V} \cdot \nabla q' \rangle$ and $\langle -\bar{\omega} \partial_p q' \rangle$ are weaker than dynamic processes, they also contributed to the extreme rainfall amounts. Evaporation *E*, for its part, contributed very little (0.1 mm/day). This is consistent with Cook et al. (2019) who found that rainfall anomalies in equatorial Central Africa do not depend directly on surface heating. It should also be noted that the residual term for a value of -1.2 mm/day is considerable. Indeed, the northward shift and strengthening of the northern component of the East African Jet (AEJ-N) in October are verified (Nicholson et al. 2022). This is illustrated by the anomalous 700 hPa zonal wind in October 2019. In addition, the anomalous variance of the band-pass filtered 700 hPa meridional wind over 2-6 days is also visible, indicating African easterly wave activity (Reed et al., 1977). Other studies also point out that rainfall fluctuations in equatorial Africa are associated with Kelvin waves (Jackson et al., 2019). The residual term could influence the estimation of dynamic and thermodynamic distributions in the water budget. Analysis of the components of the water balance over the western part of the Congo Basin (6°S-5°N, 6°-20°E) for October 2019 (Fig. 6) shows that the increase in rainfall was dominated by vertical advection of moisture induced by changes in vertical velocity $\langle -\omega' \partial_p \bar{q} \rangle$ (1.4 mm/day). However, the contributions of the other processes, including the residual term, are low.

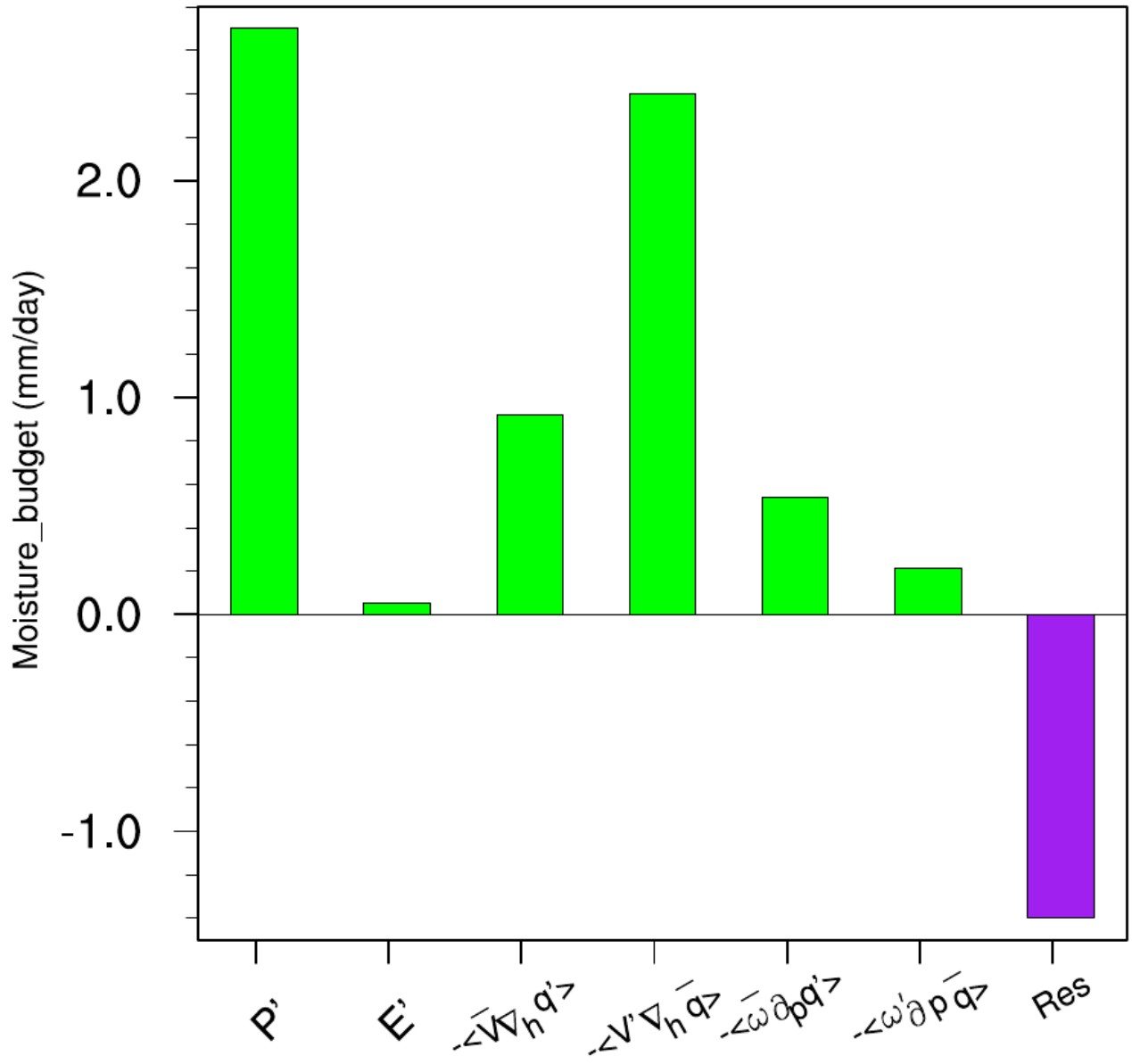

315

316 **Fig. 5** Monthly mean anomalies in moisture budget for October 2019, averaged over the Northern
317 part of West Central Africa (6°N-14°N, 6°-20°E).

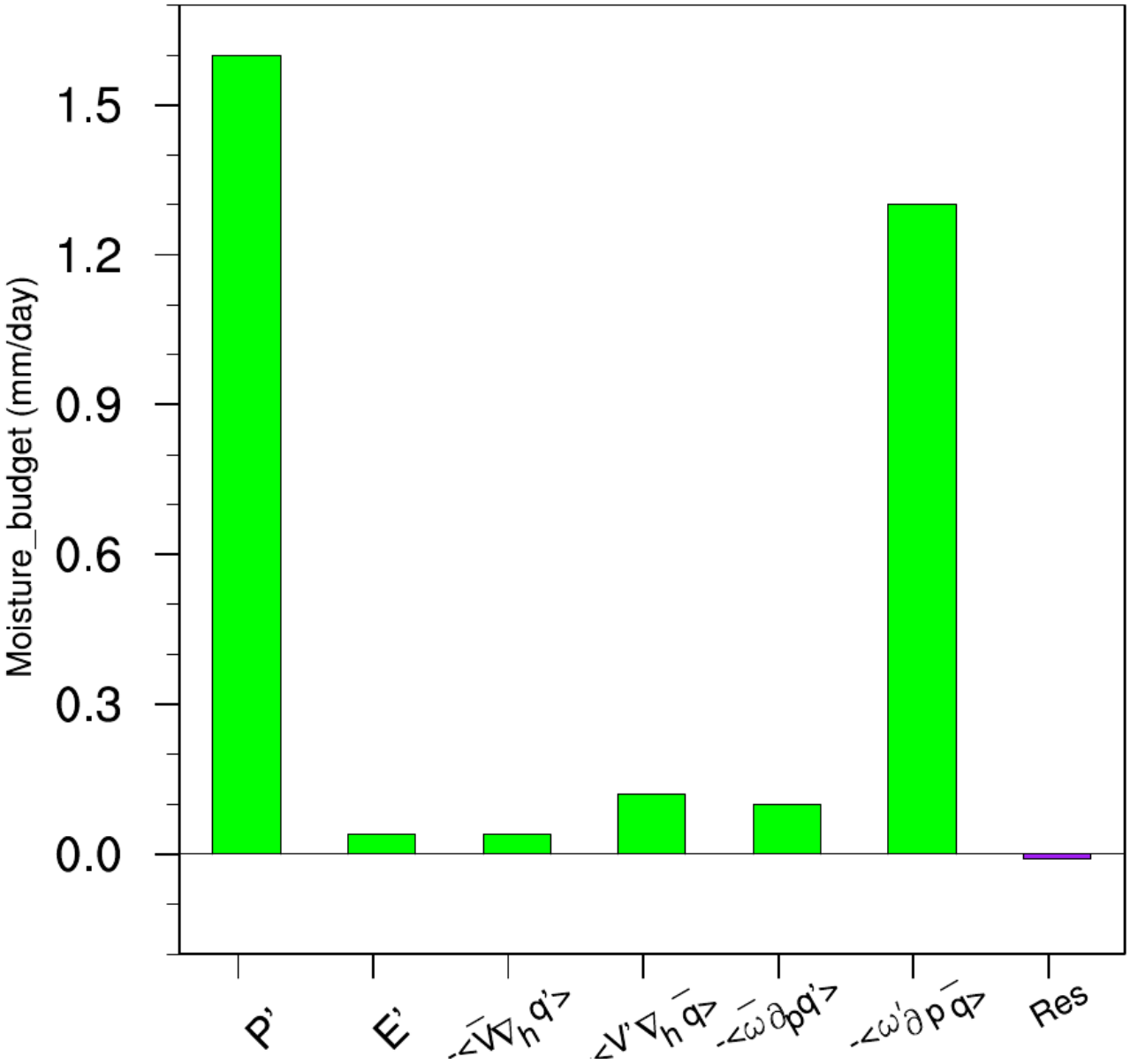

318

319 **Fig. 6**. Monthly mean anomalies in moisture budget for October 2019, averaged over the Southern
320 part of West Central Africa (6°S-5°N, 6°-20°E).

321 At the pixel scale, positive precipitation anomalies over eastern Nigeria, southern Chad and
322 northern Cameroon (Fig. 7a) were mainly dominated by horizontal moisture advection induced by
323 the horizontal wind anomaly (Fig. 7d). Over Gabon, south of Congo Brazzaville, positive
324 precipitation anomalies were dominated by vertical moisture advection induced by vertical
325 anomalous motion (Fig. 7f). Horizontal moisture advection induced by the specific humidity
326 anomaly (Fig. 7c), although not the key factor associated with precipitation patterns, shows a small
327 positive contribution over the northern part of the domain.

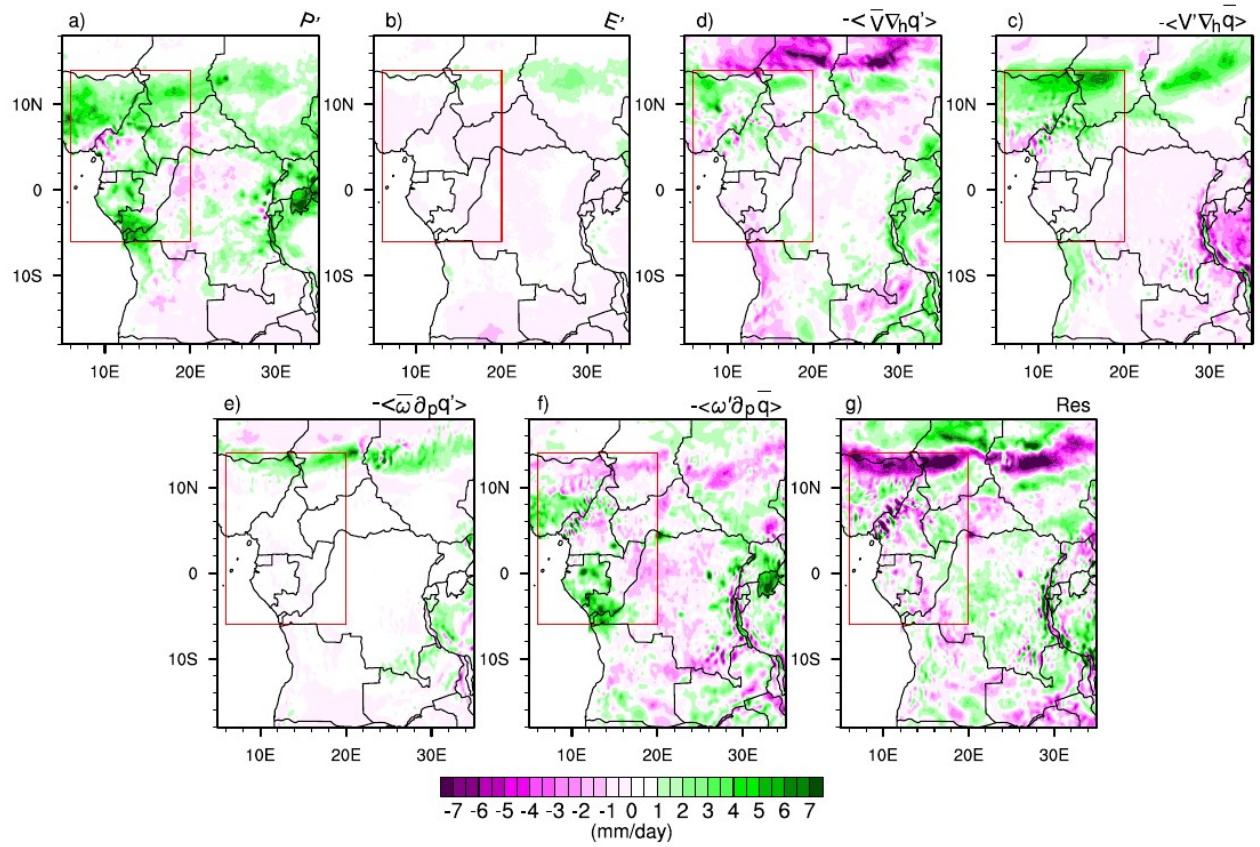

328

329 **Fig. 7**. Spatial distributions of each term of the water budget equation during October 2019 over West
330 Equatorial Africa (Red box). (a) Precipitation anomalies, (b) evaporation anomaly, (c) horizontal
331 advection of anomalous moisture by climatological wind, (d) horizontal advection of climatological
332 moisture by anomalous wind, (e) vertical advection of anomalous moisture by climatological vertical
333 velocity, (f) vertical advection of climatological moisture by anomalous vertical velocity and (g) the
334 residual term.

335

336 The contribution of evaporation (Fig. 7b) and horizontal advection of moisture induced by the
337 specific humidity anomaly (Fig. 7e) remains weak over the entire domain, although some positive
338 values can be seen around 14°N. This result is similar to that provided by MERRA2 (Figure S2).
339 Thermodynamic effects reflect the change in the thermal state of the atmosphere associated with the
340 October 2019 rainfall extremes over West Central Africa. It should be noted that changes in the
341 thermal state of the atmosphere may allow us to speculate on the potential role of global warming in
342 rainfall variations in 2019, even without considering potential impacts on atmospheric dynamics.
343 However, changes in the thermodynamic effect, although not the key factor responsible for the
344 October 2019 events, contributed up to 35% of the total effect (the sum of dynamic and
345 thermodynamic contributions) on the northern part and 15% on the southern part of the domain.

This could be since the increase in diabatic heating contributes to the change in the thermal state of the atmosphere, i.e. the increase in thermodynamic effects (changes in humidity). In fact, Nicholson et al. (2022) reported that the increase in SST in the tropical Atlantic strengthened the advection of moist air from the Atlantic towards the region, with an increase in the moisture flux from the west to southwest.

5 MSE budget analysis

The previous results clearly showed that the vertical advection of moisture induced by the vertical velocity anomaly was identified as the second dynamic parameter (after the horizontal advection of moisture induced by the anomalous horizontal movement) contributing to the increase in precipitation in October 2019. Diagnosis of the MSE budget, which takes account of the thermal state of the atmosphere and the effect of atmospheric circulation, is used to analyse the atmospheric perturbation related to moisture transport. The MSE largely influences the structure of vertical motion. In addition, diagnosis of the MSE balance emphasises the relative contributions of temperature, specific humidity and atmospheric circulation associated with the vertical motion anomaly.

The vertical profiles of the vertical velocity anomaly ω' and the MSE climatology $\bar{m}$ averaged over the north of the domain are shown in Figure 8a. The vertical velocity anomaly ω' shows positive values at the surface and negative values in the middle and upper troposphere. The alternation of positive and negative values in the tropospheric column probably reduces the contribution of the vertical advection of moisture induced by the anomalous vertical motion. The MSE climatology $\bar{m}$ exhibits a bottom-heavy bove structure with a minimum around 650 hPa. Such a structure generally indicates that $\langle \partial_p \bar{m} \rangle < 0$ (Chen and Bordoni, 2014; Liu et al. 2021; Wen et al. 2022). As a result, positive (negative) values of $\langle \omega' \partial_p \bar{m} \rangle$ depends on the vertical structure of the omega anomalies. The vertical velocity climatology $\bar{\omega}$ (Fig. 8b) is negative over the entire troposphere, characterising an upward movement. The MSE anomaly m' decreased slightly near the surface then increased from 800 hPa to 550 hPa, with a minimum value around 550 hPa. However, this includes three terms, namely, gz' which is weak in the entire tropospheric column, the enthalpy anomaly $c_p T'$, which tends to increase, and $l_v q'$,tends to behave similarly to m' between 650 hPa and 300 hPa. To the south of the domain (Fig. 8c), the vertical velocity anomaly

shows negative

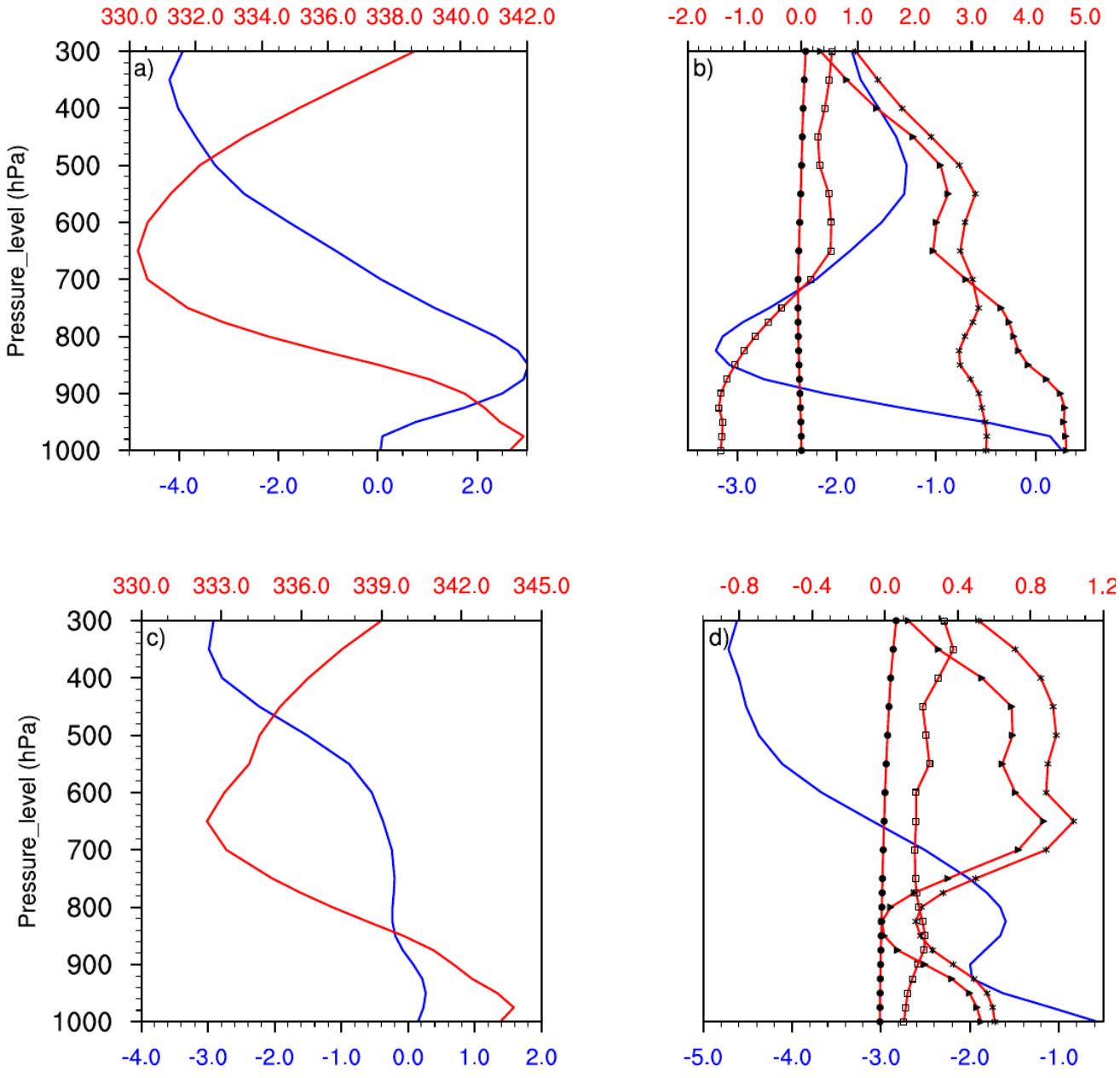

Fig. 8. Vertical profile of a) vertical velocity anomaly ω' (blue line: $10^{-2} Pa.s^{-1}$) and MSE climatology $\bar{m}$ (red line: $10^{3} J.Kg^{-1}$), and b) vertical velocity climatology $\bar{\omega}$ (blue line: $10^{-2} Pa.s^{-1}$), MSE anomaly m' (line with stars: $10^{3} J.Kg^{-1}$), enthalpy anomaly $c_p T'$ (line with

squares: $10^3 J.Kg^{-1}$), latent energy anomaly $l_v q'$ (line with triangles: $10^3 J.Kg^{-1}$) and geopotential anomaly Ψ' (line with dark circle: $10^3 J.Kg^{-1}$) averaged over the Northern part of West Central Africa (6°N-14°N, 6°-20°E) and c), d) the same parameters averaged over the Southern part of West Central Africa (6°S-5°N, 6°-20°E) during October 2019.

values from 900 hPa up to the upper troposphere, accelerating the anomalous vertical movement. The structure of the MSE climatology is similar to that observed to the north, with a maximum of around 650 hPa. The vertical profiles (Fig. 8d) of the MSE anomaly and the latent energy anomaly show similar structures throughout the tropospheric column, with maximum values at 650 hPa.

Based on the contributions of the different terms in equation 9 to the MSE over the northern part of West Central Africa (Fig. 9), the advection of wet enthalpy induced by the horizontal wind anomalies $-\langle V' \cdot \nabla \bar{M} \rangle$ is the main term contributing most to the vertical advection of the MSE induced by the vertical velocity anomaly $\langle \omega' \partial_p \bar{m} \rangle$. This is confirmed by the high correlation (r = 0.6) between the two terms compared to the other terms.

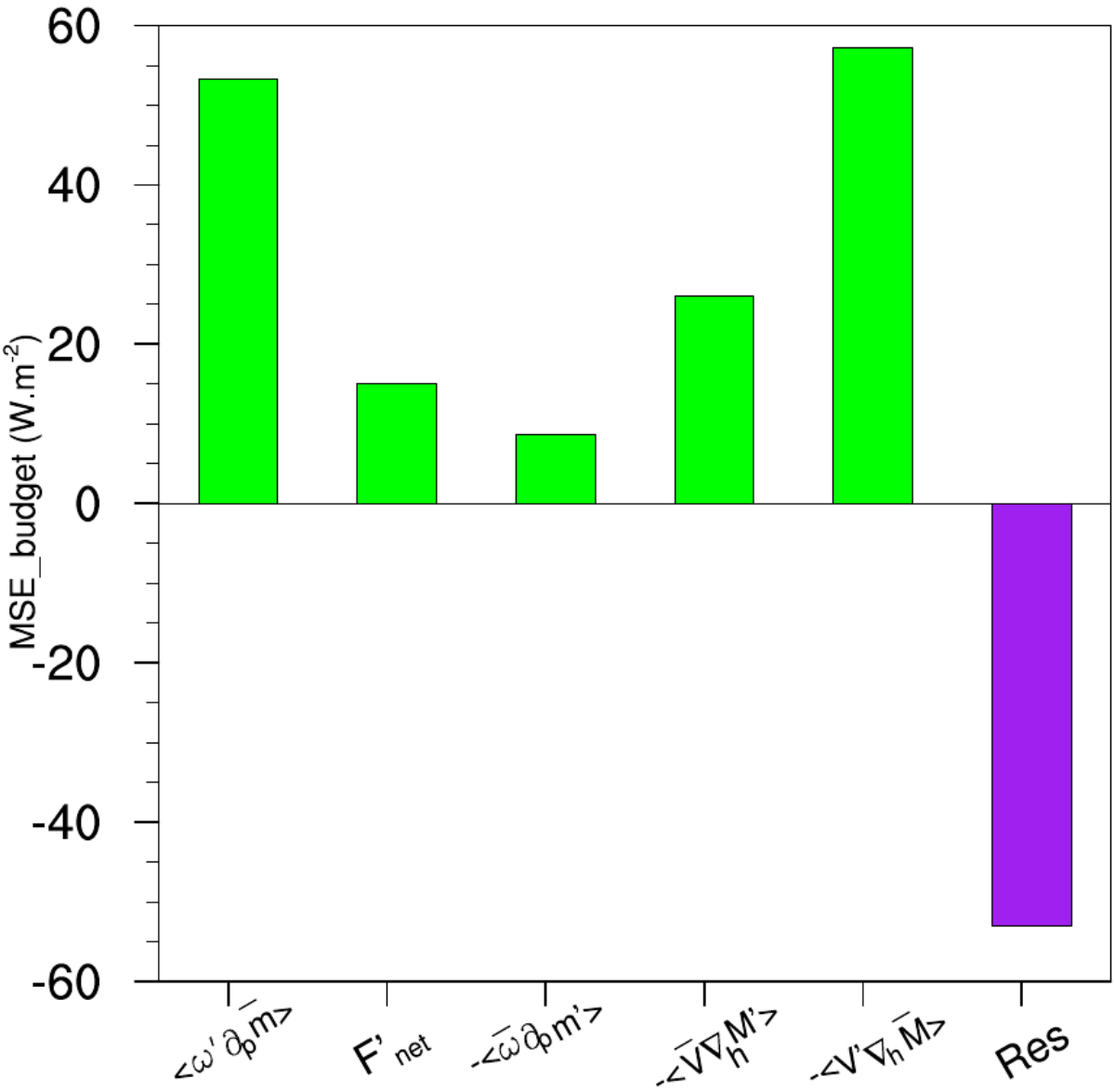

Fig. 9. Different terms of the Moist Static Energy (MSE) budget averaged over the Northern part of West Central Africa (6°N-14°N, 6°-20°E).

We also note the contribution of the thermodynamic terms, although the horizontal advection of the MSE induced by the wet enthalpy variation $-\langle \nabla \cdot \nabla M' \rangle$ dominates (r = 0.3) compared to the vertical advection of the MSE induced by the MSE variation $-\langle \omega \partial_p m' \rangle$ (r = -0.2). A weak contribution from the net flow of energy is noticeable (r = 0.18). This could be due to the fact that the energy in the radiative and turbulent heat fluxes penetrating the atmosphere over West Central Africa has suffered a loss linked to the increase in cloud cover, which has a strong influence on short-wave radiation. Such a reduction in energy in the air column has an impact on upward motion.

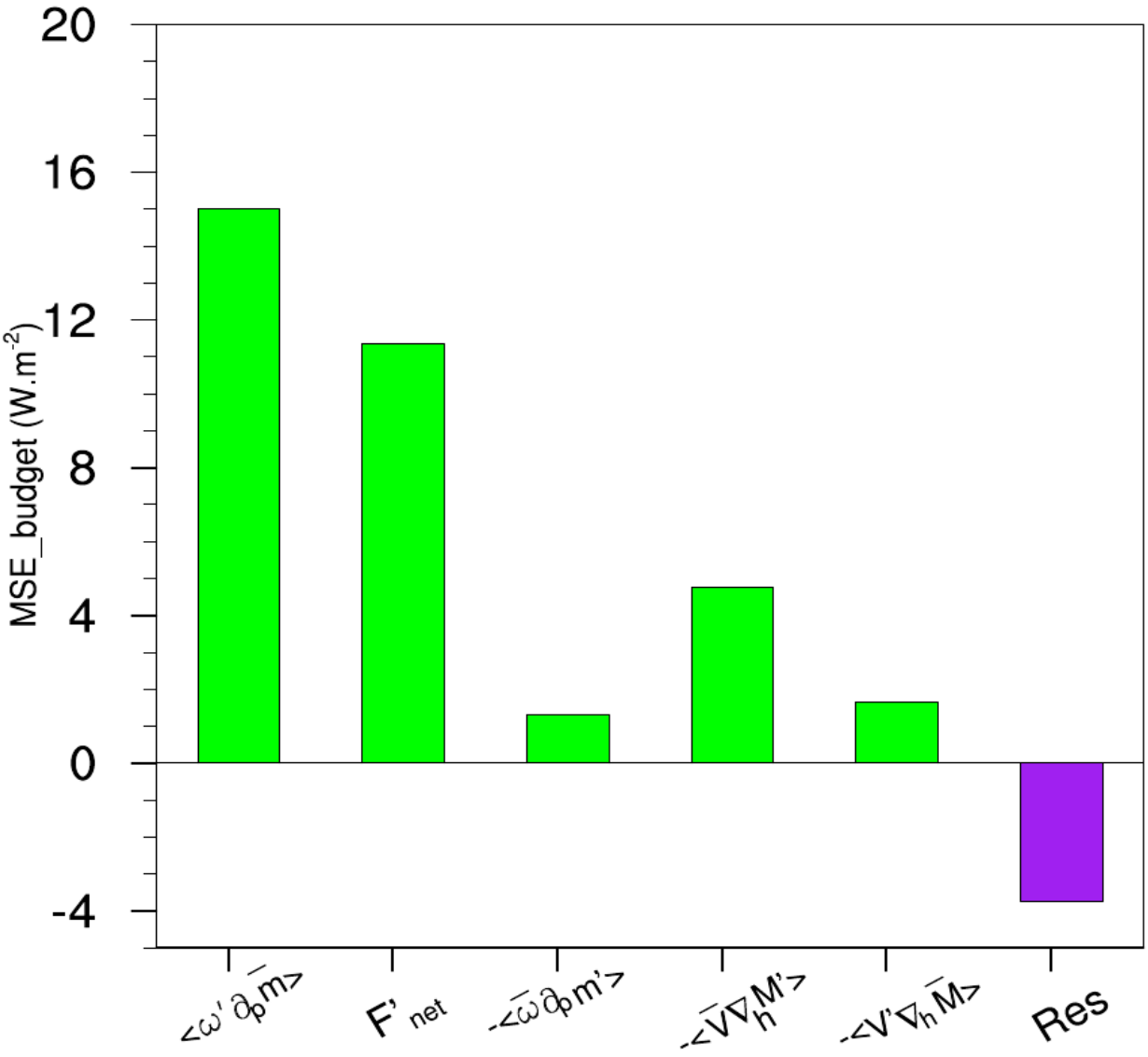

Fig. 10. Different terms of the Moist Static Energy (MSE) budget averaged over the Southern part of West Central Africa (6°S-5°N, 6°-20°E).

This result is in line with that of Wen et al. (2022) and Sheng et al. (2023), who pointed to a reduction in the net energy in the air column during the exceptional rainy season in the summer of 2020 in the Yangtze River valley and the anomalous increase in precipitation over southern China in 2022. However, as with the moisture balance, the residual term is also considerable.

To the south of the domain(Fig. 10), the increase in the net energy balance was responsible for strengthening the vertical advection of the MSE induced by the vertical velocity anomaly (r = 0.51). In addition, the increase in vertical movement was reinforced by an increase in the horizontal advection of the MSE induced by the variation in wet enthalpy $-\langle \nabla \cdot \nabla M' \rangle$. This is in agreement

with the results of Kenfack et al. (2024) who highlighted the importance of horizontal advections in the MSE and moisture flux as well as their implications for vertical motion over the Congo Basin. The contributions in vertical advection induced by changes in the MSE and horizontal advection induced by changes in the horizontal wind are small. Moreover, similarly to the moisture flux advected in the western part of the Congo Basin, the residual term was less important in the MSE budget compared to the northern part.

On a regional scale, the vertical advection of the MSE induced by the vertical motion anomaly $\langle \omega' \partial_p \bar{m} \rangle$ (Fig. 11a) is mainly dominated by the dynamic term $-\langle V' \cdot \nabla \bar{M} \rangle$ (Fig. 11c), which

427 brings moist enthalpy into the domain.

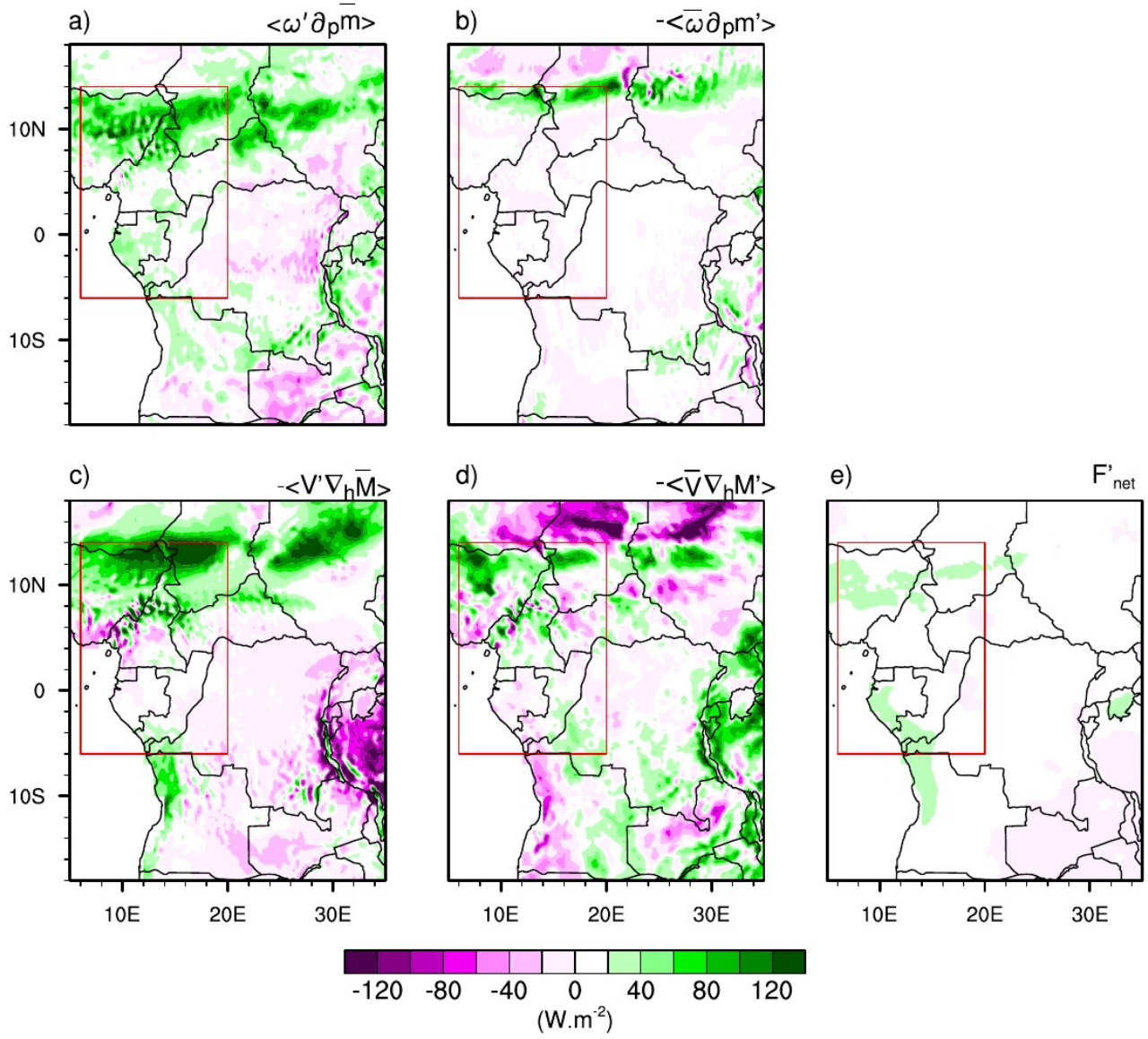

428

Fig. 11. Spatial distributions of each term of the Moist Static Energy (MSE) balance equation during October 2019 over West Equatorial Africa (Red box). (a) vertical advection of climatological MSE by anomalous vertical velocity, (b) vertical advection of anomalous MSE by climatological vertical velocity, (c) horizontal advection of anomalous moist enthalpy by climatological wind, (e) horizontal advection of climatological moist enthalpy by anomalous wind, and (f) net energy flux (at the surface and top of the atmosphere) in the atmospheric column.

There is a high concentration of positive values in both dynamic terms, up to 120 $W \cdot m^{-2}$ in the north of West Central Africa. In addition, the two thermodynamic terms $-\langle \omega \partial_p m' \rangle$ (Fig. 11b) and $-\langle \nabla \cdot \nabla M' \rangle$ (Fig. 11d), although weak, also contributed to reinforcing the vertical advection of MSE induced by the vertical motion anomaly. It should be remembered that the term $-\langle \omega \partial_p m' \rangle$ remains very weak over the region as a whole, except the northern part where a slight layer of positive values can be observed. Terms $-\langle V' \cdot \nabla \bar{M} \rangle$, $-\langle \nabla \cdot \nabla M' \rangle$ and $-\langle \omega \partial_p m' \rangle$ in the MSE have a similar spatial distribution to terms $\langle -V' \cdot \nabla \bar{q} \rangle$, $\langle -\nabla \cdot \nabla q' \rangle$ and $\langle -\bar{\omega} \partial_p q' \rangle$ in the moisture, which is in agreement with the findings of Kenfack et al. (2024). The difference between the net energy balance for 2019 and the climatology (Fig. 11e) shows low positive values in the north and south of the region respectively. Such an increase (mainly to the south of the area) is associated with a strengthening in the vertical structure of the MSE anomaly through ascending currents and, consequently, an increase in precipitation. Although the dynamic contribution is the most important, the thermodynamic contribution cannot be neglected. This would mean that the interaction between atmospheric dynamic and thermodynamic variables would induce significant indirect effects on October 2019 precipitation anomalies over West Central Africa.

5.1 Dynamic effect

The aforementioned results clearly show that enthalpy advection induced by the horizontal wind anomaly is crucial in understanding the processes at the origin of October 2019 extreme precipitation over northern part of West Central Africa. It should be remembered that, as we mentioned in the diagnostic section of the MSE balance, the wet enthalpy $M = c_p T + L_v q$ results from the sum of the dry enthalpy and the latent heat. Thus, the horizontal advection of wet enthalpy induced by the wind anomaly can be separated into two terms: dry enthalpy $-\langle V' \cdot \nabla_h c_p T \rangle$ (Fig. 12a) and latent heat $-\langle V' \cdot \nabla_h l_V \bar{q} \rangle$ (Fig. 12d).

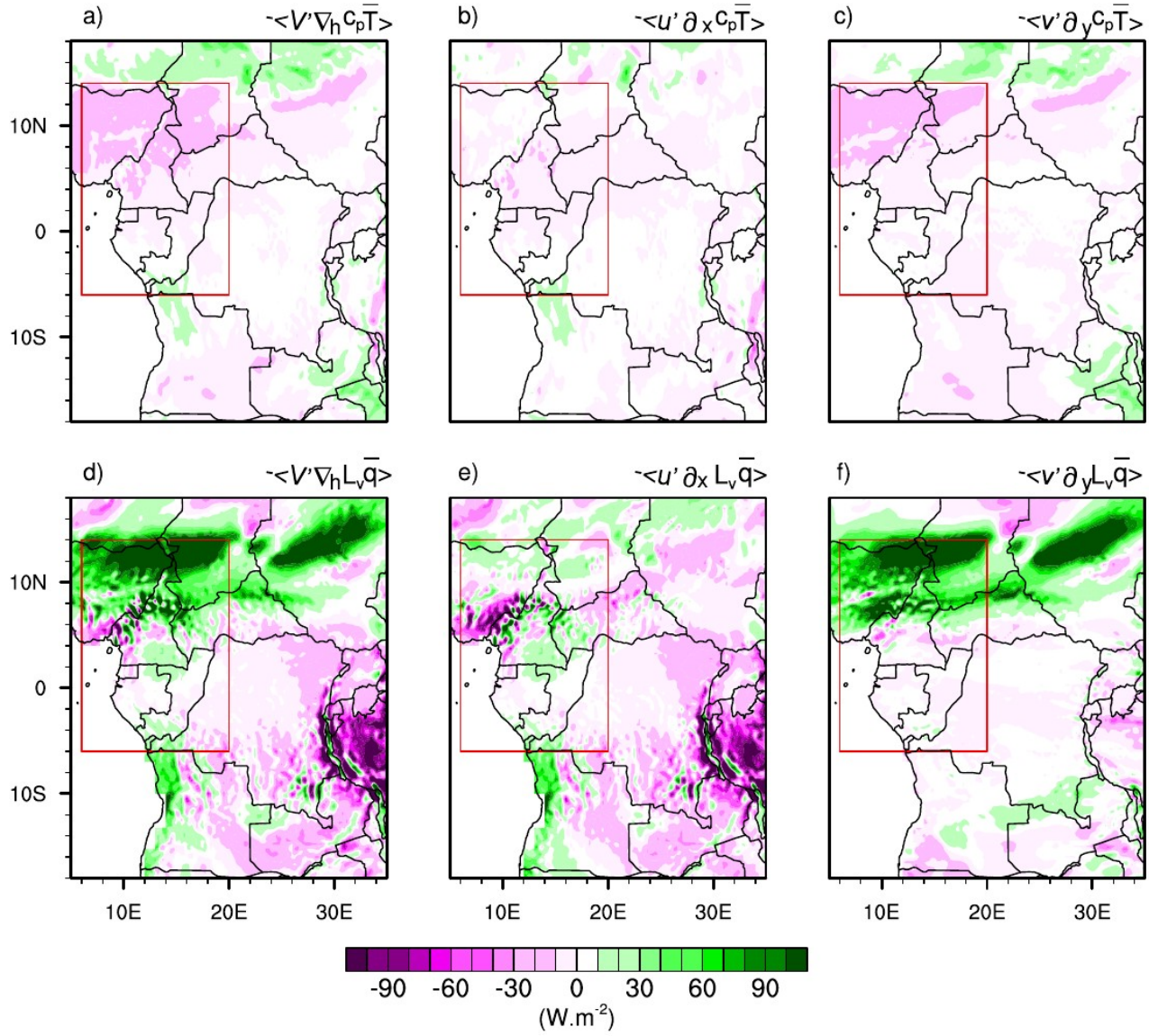

459

460 **Fig. 12**. Horizontal advection of (a–c) climatological dry enthalpy and (d–f) latent energy by
461 anomalous wind, designated as a dynamic effect during October 2019 over West Central Africa
462 (Red box). (a, d) Total advection, (b, e) zonal component, and (c, f) meridional component.

463

464 Given the influence of the wind anomaly components on the displacement of dry enthalpy and
465 latent heat, a further decomposition of the $-\langle V' \cdot \nabla_h c_p T \rangle$ and $-\langle V' \cdot \nabla_h l_v \bar{q} \rangle$ terms along the
466 zonal (Figs. 12b,e) and meridional (Figs. 12c,f) directions appear necessary. Figure 12a shows that
467 the advection of dry enthalpy induced by the horizontal wind anomaly decreased over the area-
468 averaged, with the highest values between 6°N and 14°N. The advection of dry enthalpy by the
469 meridional wind anomaly (Fig. 12c) is particularly responsible for the decrease in the

$-\langle V' \cdot \nabla_h c_p T \rangle$ term compared with the advection of dry enthalpy induced by the zonal wind anomaly (Fig. 12b), which is weak. For the transport of latent heat (Fig. 12d), the influence of the advection of $-\langle V' \cdot \nabla_h l_V \bar{q} \rangle$ term under the effect of the anomalous meridional circulation is the main term responsible for the supply of moist air to the northern part of the area, while the low contribution to the south is associated with a low input of moist air from the zonal wind anomaly (Fig. 12f). Analysis of the advection of dry enthalpy and latent heat by anomalous winds shows that the meridional wind anomaly had a significant impact compared with the zonal wind anomaly. In addition, the advection of the dynamic term associated with latent heat contributed significantly to the supply of MSE to West Central Africa compared to the advection of the dynamic term associated with dry enthalpy. One of the reasons would be because in addition to the warm Atlantic SSTs, there was also an anomalous meridional mean sea level pressure (MSLP) gradient in the Central African Sahel between a lower MSLP over the eastern Sahara and a higher pressure between 10 and 15°N. In addition, the trans-equatorial meridional wind fluctuated with the activity of the African easterly waves over the Gulf of Guinea (Nicholson et al. 2022).

5.2 Thermodynamic effect

The results of the previous section highlighted the importance of dynamics, particularly in a meridional direction, on extreme precipitation in October 2019. However, we previously also observed that the thermodynamic contribution should not be neglected. Similar to the previous section, the thermodynamic term $-\langle \bar{V} \cdot \nabla M' \rangle$ (i.e. the advection of the wet enthalpy anomaly associated with wind climatology) can also be separated into two terms, namely: Dry enthalpy $-\langle \bar{V} \cdot \nabla_h c_p T' \rangle$ (Fig. 13a) and latent heat $-\langle \bar{V} \cdot \nabla_h l_V \bar{q}' \rangle$ (Fig. 13d).

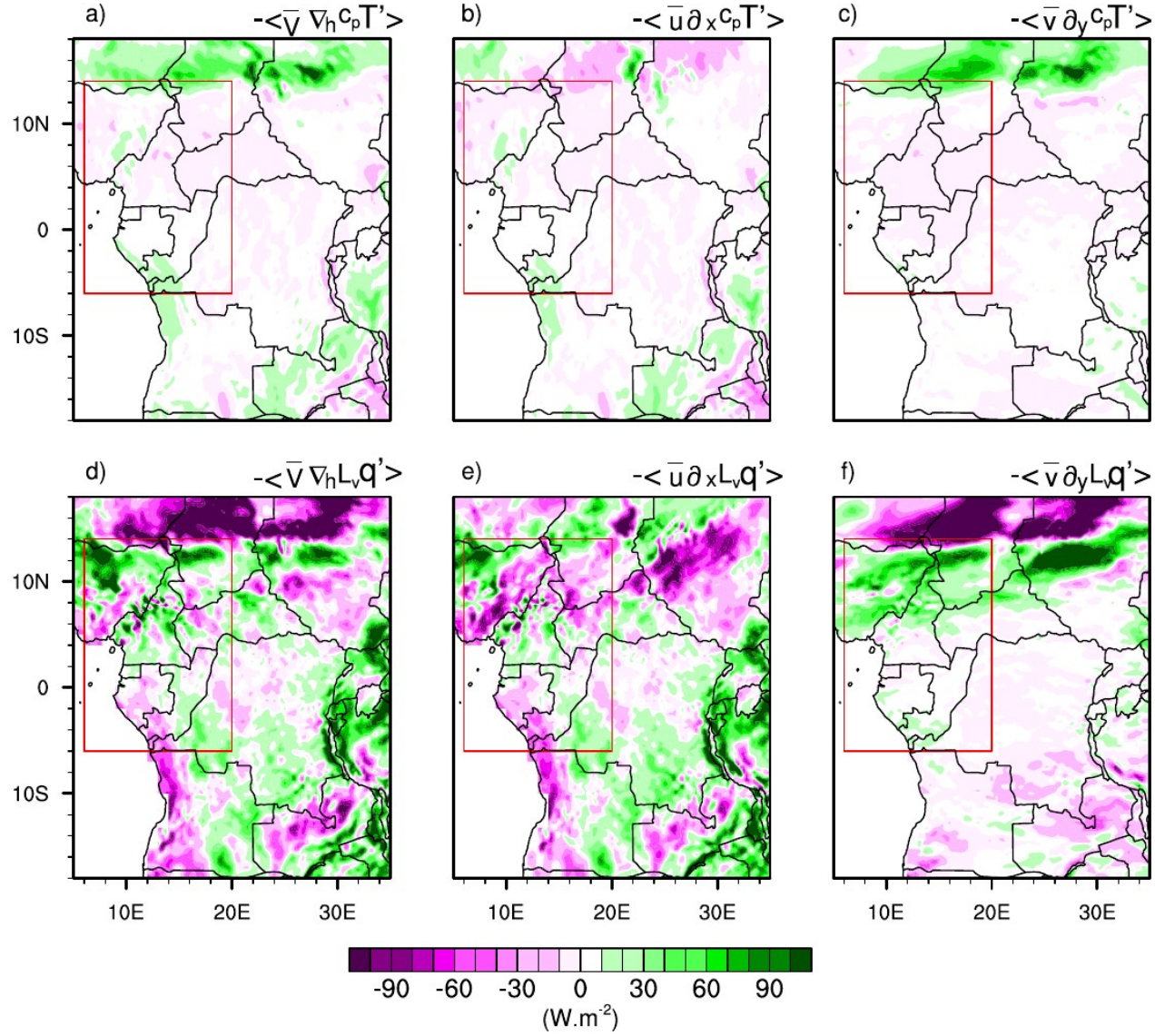

491

492 **Fig. 13.** As in Fig. 12, but for the thermodynamic effect (horizontal advection of anomalous dry
493 enthalpy and latent energy by climatological wind) during October 2019 over West Central Africa
494 (Red box).

495

496 To better assess the contribution of each term, we split the horizontal wind into zonal and
497 meridional directions. The advection of the dry enthalpy anomaly by the horizontal zonal and
498 meridional wind components is shown in Figures 13b and 13c, respectively. It can also be seen that
499 the dry enthalpy anomaly is very small over the whole area. On the other hand, the advection of the
500 latent heat anomaly by the horizontal wind climatology is more pronounced. Variations in latent
501 heat are strong in the meridional direction, while the zonal direction shows a reduction in abnormal
502 latent heat. This could be due to the strong meridional wind associated with the increase in SST in

the tropical Atlantic, which results in strong advection of water vapor into West Central Africa, leading to precipitation. The reduction in advection of the latent heat anomaly on the Atlantic coast is amplified by the zonal wind climatology. However, the advection of the wet enthalpy induced by the horizontal wind anomaly (dynamic effect) is stronger than the advection of the wet enthalpy anomaly by the wind climatology. As a result, we note in particular the changes in the meridional wind for the dynamic effect and the latent heat associated with the warming of the equatorial Atlantic for the thermodynamic effect.

6 Summary and concluding remarks

West Central Africa was hit by unprecedented exceptional rainfall in October 2019. A few studies have investigated the meteorological causes associated with these extreme rainfall events (Wainwright et al, 2020; Nicholson et al. 2022). This study followed these perspectives and focused on evaluating the dynamic and thermodynamic processes that controlled the extreme events of 2019. We proceeded by decomposing the water balance and MSE equation, separating the associated dynamic and thermodynamic effects. Changes in atmospheric circulation are behind dynamic processes, while changes in water vapor are behind thermodynamic processes. This approach provides a better understanding of the mechanisms behind rainfall anomalies. The thermodynamic effect, in particular, can be used to speculate on the influence of global warming on heavy rainfall in October 2019, notably on the increase in the temperature of the troposphere and its water vapor content. The main findings can be summarised as follows:

1. The main feature of October 2019 in the northern part of the area was a strong southerly circulation compared with the typical climatology for 1988-2017. In addition, a more pronounced rate of humidity associated with significant diabatic heating over West Central Africa up to 15°N was recorded.
2. The diagnosis of the water balance reveals that the exceptional rainfall in October 2019 was mainly dominated by dynamic effects. However, moisture advection induced by horizontal wind anomalies is the dominant process of precipitation anomalies over the northern part of the zone, while vertical moisture advection induced by vertical velocity anomalies is the dominant process of precipitation extremes in the south, mainly over Gabon and southern Congo Brazzaville. Changes in the thermodynamic effect, although not the key factor responsible for the events of October 2019, contribute up to 35% of the total effect (the sum of the dynamic and thermodynamic contributions) on the northern part and 15% on the southern part of the domain. The contribution of evaporation remains weak in both areas

combined, which allows us to conclude that evaporation was not responsible for the heavy rainfall of October 2019 in West Central Africa.

3. The MSE vertical advection anomaly is dominated over the northern part of the area by the dynamic term (i.e. the advection of the wet enthalpy induced by the horizontal wind anomalies) compared to the thermodynamic terms (i.e. the horizontal advection of the MSE induced by the variation of the wet enthalpy and the vertical advection of the MSE induced by the variation of the MSE). In the southern part, the increase in the net energy balance compared with the climatology is the dominant process that has contributed most to the change in the structure of the vertical anomaly of the MSE. An extended analysis shows that these variations in the MSE over the north of West Central Africa were governed by its meridional component, in particular the variations in the meridional wind in the dynamic effect and the meridional variations in latent heat in the thermodynamic effect. It should be pointed out that in both cases, the contribution of dry enthalpy helped to reduce the dynamic term and was small in the thermodynamic term.

The results of this study show that moisture advection induced by horizontal wind anomalies and vertical moisture advection induced by vertical velocity anomaly were crucial mechanisms in the anomalous October 2019 exceptional rainfall increase over West Central Africa. In addition, changes in the MSE budget, mainly through the meridional circulation (dynamic effect), and latent heat (thermodynamic effect) also played an important role in the northern part of the area, while the increase in the energy balance contributed considerably to the change in the MSE balance in the southern part of the area. However, there was little contribution from dry enthalpy. These results are consistent with those of Nicholson et al (2022) who showed that the increase in equatorial Atlantic SSTs associated with the late retreat of the West African monsoon played an important role in precipitation anomalies in the Sahel. Changes in SSTs along the east coast of the equatorial Atlantic display a similar pattern to the Atlantic Niño as described by Lutz et al. (2013). Furthermore, Vallès-Casanova et al (2020) also highlighted the fact that 2019 was characterised by a particularly intense Atlantic Niño, which lasted until October, placing the dynamic and thermodynamic processes in the context of the large-scale circulation. The importance of the dynamic contribution during extreme precipitation events has been reported in other regions, notably over southern China (Wen et al. 2022; Sheng et al. 2023). This calls for comprehensive evaluations of both dynamic and thermodynamic contributions, and their possible feedback, to assess the potential impact of climate change on extreme precipitation events in this region.

Acknowledgements. The authors thank all the observational and reanalysis data providers used in this study, and the research of the International Joint Laboratory “Dynamics of Terrestrial Ecosystems in Central Africa: A Context of Global Changes” (IJL DYCOCA/LMI DYCOFAC).

Competing Interests. The authors declare that they have no conflict of interest.

Authors' contributions

kevin Kenfack: Conceptualization; data analysis; formal analysis; investigation; methodology; writing - original draft; review and editing.
Francesco Marra: Supervision; conceptualization; investigation; writing – review and editing.
Zéphirin Yepdo Djomou: Investigation; writing; review and editing; supervision; validation.
Lucie A. Djiotang Tchotchou: Validation; supervision; methodology; writing – review and editing.
Alain T. Tamoffo: Conceptualization; investigation; methodology; project administration; resources; supervision; validation; review and editing.
Derbetini A. Vondou: Project administration; supervision; resources; validation; methodology; writing – review and editing.

Funding. Not applicable

Data Availability Statement

The **ERA5** reanalysis is produced within the Copernicus Climate Change Service (C3S) by the ECMWF and is accessible via the link https://cds.climate.copernicus.eu/cdsapp#!/dataset/reanalysis-era5-pressure-levels-monthly-means?tab1⁄4form.

References

Andrews, P. C., Cook, K. H., and Vizy, E. K.: Mesoscale convective systems in the Congo Basin: Seasonality, regionality, and diurnal cycles, Clim. Dynam., 62, 609–630, https://doi.org/10.1007/s00382-023-06903-7, 2023.

Kenya – over 100 dead, 18,000 displaced after recent floods and landslides – floodlist: http://floodlist.com/africa/kenya-floods-november-2019, last access: 2 April 2024.

Aretouyap, Z., Kemgang, F. E. G., Domra, J. K., Bisso, D., and Njandjock, P. N.: Understanding the occurrences of fault and landslide in the region of West-Cameroon using remote sensing and GIS techniques, Nat. Hazards, 109, 1589–1602, https://doi.org/10.1007/s11069-021-04890-8, 2021.

Bell, J. P., Tompkins, A. M., Bouka-Biona, C., and Sanda, I. S.: A process-based investigation into the impact of the Congo basin deforestation on surface climate, J. Geophys. Res-Atmos., 120, 5721–5739, https://doi.org/10.1002/2014jd022586, 2015.

Black, E.: The relationship between Indian Ocean sea–surface temperature and East African rainfall, Philos. T. R. Soc. A, 363, 43–47, https://doi.org/10.1098/rsta.2004.1474, 2005.

Chadwick, R., Good, P., and Willett, K.: A simple moisture advection model of specific humidity change over land in response to SST warming, J. Climate, 29, 7613–7632, https://doi.org/10.1175/jcli-d-16-0241.1, 2016.

Chen, J. and Bordoni, S.: Orographic effects of the Tibetan plateau on the east Asian summer monsoon: An energetic perspective, J. Climate, 27, 3052–3072, https://doi.org/10.1175/jcli-d-13-00479.1, 2014.

Cook, K. H. and Vizy, E. K.: Hydrodynamics of regional and seasonal variations in Congo Basin precipitation, Clim. Dynam., 59, 1775–1797, https://doi.org/10.1007/s00382-021-06066-3, 2021.

Cook, K. H., Liu, Y., and Vizy, E. K.: Congo Basin drying associated with poleward shifts of the African thermal lows, Clim. Dynam., 54, 863–883, https://doi.org/10.1007/s00382-019-05033-3, 2019.

Dyer, E. L. E., Jones, D. B. A., Nusbaumer, J., Li, H., Collins, O., Vettoretti, G., and Noone, D.: Congo Basin precipitation: Assessing seasonality, regional interactions, and sources of moisture, J. Geophys. Res-Atmos., 122, 6882–6898, https://doi.org/10.1002/2016jd026240, 2017.

Fontaine, B., Roucou, P., and Trzaska, S.: Atmospheric water cycle and moisture fluxes in the West

African monsoon: Mean annual cycles and relationship using NCEP/NCAR reanalysis, Geophys. Res. Lett., 30, https://doi.org/10.1029/2002gl015834, 2003.

Fotso-Nguemo, T. C., Chamani, R., Yepdo, Z. D., Sonkoué, D., Matsaguim, C. N., Vondou, D. A., and Tanessong, R. S.: Projected trends of extreme rainfall events from CMIP5 models over Central Africa, Atmos. Sci. Lett., 19, https://doi.org/10.1002/asl.803, 2018.

Fotso-Nguemo, T. C., Diallo, I., Diakhaté, M., Vondou, D. A., Mbaye, M. L., Haensler, A., Gaye, A. T., and Tchawoua, C.: Projected changes in the seasonal cycle of extreme rainfall events from CORDEX simulations over Central Africa, Climatic. Change, 155, 339–357, https://doi.org/10.1007/s10584-019-02492-9, 2019.

Funk, C., Peterson, P., Landsfeld, M., Pedreros, D., Verdin, J., Shukla, S., Husak, G., Rowland, J., Harrison, L., Hoell, A., and Michaelsen, J.: The climate hazards infrared precipitation with stations—a new environmental record for monitoring extremes, Scientific Data, 2, https://doi.org/10.1038/sdata.2015.66, 2015.

Garcin, Y., Deschamps, P., Ménot, G., de Saulieu, G., Schefuß, E., Sebag, D., Dupont, L. M., Oslisly, R., Brademann, B., Mbusnum, K. G., Onana, J.-M., Ako, A. A., Epp, L. S., Tjallingii, R., Strecker, M. R., Brauer, A., and Sachse, D.: Early anthropogenic impact on Western Central African rainforests 2,600 y ago, P. Natl. A. Sci. India. A, 115, 3261–3266, https://doi.org/10.1073/pnas.1715336115, 2018.

Gou, Y., Balling, J., De Sy, V., Herold, M., De Keersmaecker, W., Slagter, B., Mullissa, A., Shang, X., and Reiche, J.: Intra-annual relationship between precipitation and forest disturbance in the African rainforest, Environ. Res. Lett., 17, 044044, https://doi.org/10.1088/1748-9326/ac5ca0, 2022.

Harris, I., Osborn, T. J., Jones, P., and Lister, D.: Version 4 of the CRU TS monthly high-resolution gridded multivariate climate dataset, Scientific Data, 7, https://doi.org/10.1038/s41597-020-0453-3, 2020.

He, Y., Tian, W., Huang, J., Wang, G., Ren, Y., Yan, H., Yu, H., Guan, X., and Hu, H.: The mechanism of increasing summer water vapor over the Tibetan plateau, J. Geophys. Res-Atmos., 126, https://doi.org/10.1029/2020jd034166, 2021.

Hersbach, H., Bell, B., Berrisford, P., Hirahara, S., Horányi, A., Muñoz-Sabater, J., Nicolas, J., Peubey, C., Radu, R., Schepers, D., Simmons, A., Soci, C., Abdalla, S., Abellan, X., Balsamo, G., Bechtold, P., Biavati, G., Bidlot, J., Bonavita, M., De Chiara, G., Dahlgren, P., Dee, D., Diamantakis, M., Dragani, R., Flemming, J., Forbes, R., Fuentes, M., Geer, A., Haimberger, L., Healy, S., Hogan, R. J., Hólm, E., Janisková, M., Keeley, S., Laloyaux, P., Lopez, P., Lupu, C., Radnoti, G., de Rosnay, P., Rozum, I., Vamborg, F., Villaume, S., and Thépaut, J.: The ERA5 global reanalysis, Q. J. Roy. Meteor. Soc., 146, 1999–2049, https://doi.org/10.1002/qj.3803, 2020.

Hua, W., Zhou, L., Nicholson, S. E., Chen, H., and Qin, M.: Assessing reanalysis data for understanding rainfall climatology and variability over Central Equatorial Africa, Clim. Dynam., 53, 651–669, https://doi.org/10.1007/s00382-018-04604-0, 2019.

Huffman, G. J., Adler, R. F., Bolvin, D. T., and Gu, G.: Improving the global precipitation record: GPCP Version 2.1, Geophys. Res. Lett., 36, https://doi.org/10.1029/2009gl040000, 2009.

Jackson, B., Nicholson, S. E., and Klotter, D.: Mesoscale convective systems over Western Equatorial Africa and their relationship to large-scale circulation, Mon. Weather. Rev., 137, 1272–1294, https://doi.org/10.1175/2008mwr2525.1, 2009.

Jiang, J., Zhou, T., Chen, X., and Zhang, L.: Future changes in precipitation over Central Asia based on CMIP6 projections, Environ. Res. Lett., 15, 054009, https://doi.org/10.1088/1748-9326/ab7d03, 2020.

Johannsen, Ermida, Martins, Trigo, Nogueira, and Dutra: Cold bias of ERA5 summertime daily maximum land surface temperature over Iberian Peninsula, Remote. Sens-Basel, 11, 2570, https://doi.org/10.3390/rs11212570, 2019.

Kamae, Y., Mei, W., and Xie, S.-P.: Climatological relationship between warm season atmospheric rivers and heavy rainfall over East Asia, J. Meteorol. Soc. Jpn., Ser. II, 95, 411–431, https://doi.org/10.2151/jmsj.2017-027, 2017.

Kenfack, K., Tamoffo, A. T., Djiotang Tchotchou, L. A., and Vondou, D. A.: Assessment of uncertainties in reanalysis datasets in reproducing thermodynamic mechanisms in the moisture

budget’s provision in the Congo Basin, Theor. Appl. Climatol., 154, 613–626, https://doi.org/10.1007/s00704-023-04576-0, 2023.

Kenfack, K., Tamoffo, A. T., Tchotchou, L. A. D., Marra, F., Kaissassou, S., Nana, H. N., and Vondou, D. A.: Processes behind the decrease in Congo Basin precipitation during the rainy seasons inferred from ERA-5 reanalysis, Int. J. Climatol., https://doi.org/10.1002/joc.8410, 2024.

Kuete, G., Pokam Mba, W., and Washington, R.: African Easterly Jet South: Control, maintenance mechanisms and link with Southern subtropical waves, Clim. Dynam., 54, 1539–1552, https://doi.org/10.1007/s00382-019-05072-w, 2019.

Li, P., Zhou, T., and Chen, X.: Water vapor transport for spring persistent rains over southeastern China based on five reanalysis datasets, Clim. Dynam., 51, 4243–4257, https://doi.org/10.1007/s00382-017-3680-3, 2017.

Liu, S., Wen, N., and Li, L.: Dynamic and thermodynamic contributions to Northern China dryness in El Niño developing summer, Int. J. Climatol., 41, 2878–2890, https://doi.org/10.1002/joc.6995, 2021.

Longandjo, G.-N. T. and Rouault, M.: Revisiting the seasonal cycle of rainfall over Central Africa, J. Climate, 37, 1015–1032, https://doi.org/10.1175/jcli-d-23-0281.1, 2024.

Lutz, K., Rathmann, J., and Jacobeit, J.: Classification of warm and cold water events in the eastern tropical Atlantic Ocean, Atmos. Sci. Lett., 14, 102–106, https://doi.org/10.1002/asl2.424, 2013.

Mariotti, L., Diallo, I., Coppola, E., and Giorgi, F.: Seasonal and intraseasonal changes of African monsoon climates in 21st century CORDEX projections, Climatic. Change, 125, 53–65, https://doi.org/10.1007/s10584-014-1097-0, 2014.

Marra, F., Levizzani, V., and Cattani, E.: Changes in extreme daily precipitation over Africa: Insights from a non-asymptotic statistical approach, J. Hydrol. X, 16, 100130, https://doi.org/10.1016/j.hydroa.2022.100130, 2022.

Moon, S. and Ha, K.-J.: Future changes in monsoon duration and precipitation using CMIP6, NPJ Clim. Atmos. S., 3, https://doi.org/10.1038/s41612-020-00151-w, 2020.

Moudi Pascal, I., Kammalac Jores, T., Talib, J., Appolinaire, V. D., Hirons, L., Christian, N., Tene Romeo-Ledoux, D., Fogang Michael, T., Marceline, M., Tanessong Roméo, S., Dione, C., Thompson, E., Salih, A. A. M., and Ngaryamgaye, S.: Strengthening weather forecast and dissemination capabilities in Central Africa: Case assessment of intense flooding in January 2020, Climate Services, 32, 100411, https://doi.org/10.1016/j.cliser.2023.100411, 2023.

Nana, H. N., Tanessong, R. S., Tchotchou, L. A. D., Tamoffo, A. T., Moihamette, F., and Vondou, D. A.: Influence of strong South Atlantic Ocean Dipole on the Central African rainfall's system, Clim. Dynam., 62, 1–16, https://doi.org/10.1007/s00382-023-06892-7, 2023.

Neelin, J. D.: Moist dynamics of tropical convection zones in monsoons, teleconnections, and global warming, in: The Global Circulation of the Atmosphere, Princeton University Press, 267–301, 2021.

Ngandam Mfondoum, A. H., Wokwenmendam Nguet, P., Mefire Mfondoum, J. V., Tchindjang, M., Hakdaoui, S., Cooper, R., Gbetkom, P. G., Penaye, J., Bekoa, A., and Moudioh, C.: Adapting sudden landslide identification product (SLIP) and detecting real-time increased precipitation (DRIP) algorithms to map rainfall-triggered landslides in Western Cameroon highlands (Central-Africa), Geoenvironmental Disasters, 8, https://doi.org/10.1186/s40677-021-00189-9, 2021.

Nicholson, S. E., Fink, A. H., Funk, C., Klotter, D. A., and Satheesh, A. R.: Meteorological causes of the catastrophic rains of October/November 2019 in equatorial Africa, Global. Planet. Change, 208, 103687, https://doi.org/10.1016/j.gloplacha.2021.103687, 2022.

Oueslati, B., Yiou, P., and Jézéquel, A.: Revisiting the dynamic and thermodynamic processes driving the record-breaking January 2014 precipitation in the southern UK, Sci. Rep-Uk., 9, https://doi.org/10.1038/s41598-019-39306-y, 2019.

Pokam, W. M., Djiotang, L. A. T., and Mkankam, F. K.: Atmospheric water vapor transport and recycling in Equatorial Central Africa through NCEP/NCAR reanalysis data, Clim. Dynam., 38, 1715–1729, https://doi.org/10.1007/s00382-011-1242-7, 2011.

Pokam, W. M., Bain, C. L., Chadwick, R. S., Graham, R., Sonwa, D. J., and Kamga, F. M.: Identification of processes driving low-level westerlies in West Equatorial Africa, J. Climate, 27, 4245–4262, https://doi.org/10.1175/jcli-d-13-00490.1, 2014.

Seager, R., Naik, N., and Vecchi, G. A.: Thermodynamic and dynamic mechanisms for large-scale changes in the hydrological cycle in response to global warming*, J. Climate, 23, 4651–4668, https://doi.org/10.1175/2010jcli3655.1, 2010.

Sheng, B., Wang, H., Li, H., Wu, K., and Li, Q.: Thermodynamic and dynamic effects of anomalous dragon boat water over South China in 2022, Weather and Climate Extremes, 40, 100560, https://doi.org/10.1016/j.wace.2023.100560, 2023.

Sonkoué, D., Monkam, D., Fotso-Nguemo, T. C., Yepdo, Z. D., and Vondou, D. A.: Evaluation and projected changes in daily rainfall characteristics over Central Africa based on a multi-model ensemble mean of CMIP5 simulations, Theor. Appl. Climatol., 137, 2167–2186, https://doi.org/10.1007/s00704-018-2729-5, 2018.

Taguela, T. N., Pokam, W. M., and Washington, R.: Rainfall in uncoupled and coupled versions of the Met Office Unified Model over Central Africa: Investigation of processes during the September–November rainy season, Int. J. Climatol., 42, 6311–6331, https://doi.org/10.1002/joc.7591, 2022.

Tamoffo, A. T., Vondou, D. A., Pokam, W. M., Haensler, A., Yepdo, Z. D., Fotso-Nguemo, T. C., Tchotchou, L. A. D., and Nouayou, R.: Daily characteristics of Central African rainfall in the REMO model, Theor. Appl. Climatol., 137, 2351–2368, https://doi.org/10.1007/s00704-018-2745-5, 2019.

Tamoffo, A. T., Weber, T., Akinsanola, A. A., and Vondou, D. A.: Projected changes in extreme rainfall and temperature events and possible implications for Cameroon’s socio-economic sectors, Meteorol. Appl., 30, https://doi.org/10.1002/met.2119, 2023.

Vallès-Casanova, I., Lee, S., Foltz, G. R., and Pelegrí, J. L.: On the Spatiotemporal Diversity of Atlantic Niño and Associated Rainfall Variability Over West Africa and South America, Geophys. Res. Lett., 47, https://doi.org/10.1029/2020gl087108, 2020.

Wainwright, C. M., Finney, D. L., Kilavi, M., Black, E., and Marsham, J. H.: Extreme rainfall in East Africa, October 2019–January 2020 and context under future climate change, Weather, 76, 26–31, https://doi.org/10.1002/wea.3824, 2020.

Wang, L. and Li, T.: Effect of vertical moist static energy advection on MJO eastward propagation: Sensitivity to analysis domain, Clim. Dynam., 54, 2029–2039, https://doi.org/10.1007/s00382-019-05101-8, 2020a.

Wang, T. and Li, T.: Diagnosing the column-integrated moist static energy budget associated with the northward-propagating boreal summer intraseasonal oscillation, Clim. Dynam., 54, 4711–4732, https://doi.org/10.1007/s00382-020-05249-8, 2020b.

Wantim, M. N., Ughe, W. G., Kwah, D. C., Bah, T. C., Quinette, N., and Ayonghe, S. N.: Forensic investigation of the Gouache landslide disaster, Western Region, Cameroon, Journal of the Cameroon Academy of Sciences, 19, 223–240, https://doi.org/10.4314/jcas.v19i3.3, 2023.

Washington, R., James, R., Pearce, H., Pokam, W. M., and Moufouma-Okia, W.: Congo Basin rainfall climatology: Can we believe the climate models?, Philos. T. R. Soc. B., 368, 20120296, https://doi.org/10.1098/rstb.2012.0296, 2013.

Wen, N., Liu, S., and Li, L. Z. X.: Diagnosing the dynamic and thermodynamic effects for the exceptional 2020 summer rainy season in the Yangtze River Valley, J. Meteorol. Res-Prc., 36, 26–36, https://doi.org/10.1007/s13351-022-1126-2, 2022.

Yanai, M. and Tomita, T.: Seasonal and interannual variability of atmospheric heat sources and moisture sinks as determined from NCEP–NCAR reanalysis, J. Climate, 11, 463–482, https://doi.org/10.1175/1520-0442(1998)011<0463:saivoa>2.0.co;2, 1998.

Zhao, D., Zhang, L., and Zhou, T.: Detectable anthropogenic forcing on the long-term changes of summer precipitation over the Tibetan Plateau, Clim. Dynam., 59, 1939–1952, https://doi.org/10.1007/s00382-022-06189-1, 2022.

Zhou, L., Tian, Y., Myneni, R. B., Ciais, P., Saatchi, S., Liu, Y. Y., Piao, S., Chen, H., Vermote, E. F., Song, C., and Hwang, T.: Widespread decline of Congo rainforest greenness in the past decade,

Nature, 509, 86–90, https://doi.org/10.1038/nature13265, 2014.